JOURNAL OF GEOPHYSICAL RESEARCH, VOL. 105, NO. D18, PAGES 22,919–22,935, SEPTEMBER 27, 2000

Vertical photon transport in cloud remote sensing problems

S. Platnick

Joint Center for Earth Systems Technology, University of Maryland Baltimore County, Baltimore, Maryland
NASA Goddard Space Flight Center, Greenbelt, Maryland

Abstract. Photon transport in plane-parallel, vertically inhomogeneous clouds is investigated and applied to cloud remote sensing techniques that use solar reflectance or transmittance measurements for retrieving droplet effective radius. Transport is couched in terms of weighting functions which approximate the relative contribution of individual layers to the overall retrieval. Two vertical weightings are investigated, including one based on the average number of scatterings encountered by reflected and transmitted photons in any given layer. A simpler vertical weighting, based on the maximum penetration of reflected photons, proves useful for solar reflectance measurements. These weighting functions are highly dependent on droplet absorption and solar/viewing geometry. A superposition technique, using adding/doubling radiative transfer procedures, is used to accurately determine both weightings, avoiding time-consuming Monte Carlo methods. Effective radius retrievals from modeled vertically structured liquid water clouds are then made using the standard near-infrared bands and compared with size estimates based on the proposed weighting functions. Agreement between the two methods is generally within several tenths of a micrometer, much better than expected retrieval accuracy. Though the emphasis is on photon transport in clouds, the derived weightings can be applied to any multiple-scattering plane-parallel radiative transfer problem, including arbitrary combinations of cloud, aerosol, and gas layers.

1. Introduction

Cloud droplet size is an important parameter in physical and radiative cloud process studies, climate modeling, and investigations of potential cloud-climate feedbacks [cf. *Wielicki et al.*, 1995, for review]. For example, droplet size is influenced by both droplet concentration and water content. Droplet concentration is in turn affected by cloud condensation nuclei concentrations present during nucleation, providing a link between droplet sizes and cloud albedo via the so-called indirect effect of aerosols on climate mechanism and cloud susceptibility [*Twomey*, 1974; *Charlson et al.*, 1987; *Twomey*, 1991]. The influence of droplet concentration on precipitation processes and subsequent consequences to cloud fraction and lifetime is also of interest [*Albrecht*, 1989; *Pincus and Baker*, 1994; *Austin et al.*, 1995]. In general circulation models (GCMs), droplet size is used for the parameterization of cloud optical thickness from liquid water path. Several studies have shown GCM radiation budgets to be sensitive to droplet size due to this parameterization [*Slingo*, 1990; *Kiehl*, 1994]. All of these issues have helped spur interest in the remote sensing of cloud droplet size.

In radiative studies it is the effective radius ($r_e = \overline{r^3}/\overline{r^2}$) which is the important measure of the droplet size distribution. Solar reflectance measurements in visible and near-infrared atmospheric window bands can be used to infer cloud optical thickness and effective radius. The droplet size information is obtained with one of the water-absorbing near-infrared bands, usually located in the 1.6, 2.2, or 3.7 μm spectral region. These retrievals presume the existence of homogeneous, plane-parallel clouds, in which case, retrievals made with each near-infrared band should report the same droplet effective radii. However, both theory and in situ measurements show clouds to exhibit a measurable droplet size vertical structure; measurements and satellite imagery also indicate horizontal inhomogeneities over many scales [e.g., *Cahalan and Snider*, 1989; *Gerber et al.*, 1994]. Since transport will be shown to be highly dependent on the amount of liquid water absorption in the band, inhomogeneous clouds may lead to differences among the individual near-infrared retrievals. Retrievals using an airborne imaging radiometer flown over marine stratocumulus clouds have shown that significant differences can occur among the three near-infrared bands [*Platnick et al.*, 2000]. Though fundamental sources of retrieval error may have been responsible (e.g., instrument calibration), it is possible that cloud inhomogeneities were a contributing factor. In investigating cloud retrieval sensitivity to inhomogeneities, it is convenient to consider the vertical and horizontal scales separately. Approximations for horizontal transport have been developed for determining the horizontal extent required for size retrievals based on plane-parallel models and for providing a quantitative means for excluding cloud regions (e.g., near boundaries) from retrieval analysis to limit potential biases [*Platnick*, 2000a]. In the current work we investigate vertical photon transport in plane-parallel, vertically inhomogeneous clouds with direct application to cloud remote sensing problems that use solar reflectance or transmittance measurements to infer droplet size. This is an extension to an earlier preliminary work [*Platnick*, 1997].

It is useful in remote sensing problems to couch vertical transport through plane-parallel layers in terms of a weighting function which approximates the relative information content of each layer to the overall reflected or transmitted signal. For cloud remote sensing, this primarily means information regarding layer droplet size (related to droplet absorption).

Paper number 2000JD900333.
0148-0227/00/2000JD900333$09.00

Though weighting functions in single-scattering problems are exact, any weighting for a multiple-scattering problem can only be approximate. Several weightings are investigated, including one based on the average number of scatterings encountered by reflected and transmitted photons in any given layer. A superposition technique, using basic adding/doubling radiative transfer procedures, is used to accurately and quickly determine the number of layer scatterings, avoiding time-consuming Monte Carlo calculations. A simpler vertical weighting based on the maximum depth achieved by reflected photons proves useful for solar reflectance measurements.

We begin in section 2 with a discussion of the physics behind cloud droplet size retrievals and the basic implementation of the algorithm which presupposes homogeneous clouds. Analytic models are then developed for prescribing cloud droplet size as a function of cloud height or optical depth in section 3. These cloud models are used in later sections for assessing the effect of various droplet size profiles on retrievals and weighting functions. Candidate vertical weighting functions are proposed and discussed in section 4. Example calculations of the weighting functions are made for bidirectional and flux remote measurements and compared with Monte Carlo results. In section 5, retrievals made with the three near-infrared bands are presented for several cloud models and compared with size estimates based on the weighting functions. Conclusions regarding the impact of vertical structure on retrievals can then be made. The possibility of inferring the droplet size profile from the three retrievals via an inversion technique is discussed in section 6.

2. Cloud Microphysical Retrievals

Simultaneous cloud microphysical and optical thickness retrievals using solar reflectance measurements, along with in situ validations, began with *Twomey and Cocks* [1982, 1989], *Foot* [1988], *Nakajima and King* [1990], and *Nakajima et al.* [1991]. Though the physical basis for these retrievals is important in understanding the effects of photon transport, only a summary will be attempted here. Typical retrieval algorithms make use of multispectral information contained in bands that are absorbing and nonabsorbing for cloud particles. Since useful bands are located in atmospheric windows to minimize the effect of molecular absorption, further mention of absorption will be understood to refer to water particles and not water vapor or other gases. Though we limit our discussion to clouds with liquid water droplets, the algorithms can, at least in principle, also be applied to ice clouds [e.g., *Ou et al.*, 1995; *Young et al.*, 1998].

Nonabsorbing bands include atmospheric windows from the visible up to effectively 1.2 μm, each with particular advantages depending on underlying surface type. Reflectance in these bands depends primarily on cloud optical thickness, with only a small droplet size dependence through the scattering asymmetry parameter. Unless otherwise stated, reflectance will refer to the bidirectional quantity (i.e., a function of both solar and viewing directions) and not albedo, or hemispheric flux reflectance. For conservative scattering, cloud reflectance increases monotonically with optical thickness toward a limiting value near unity, though not necessarily exact unity for bidirectional reflectance.

The useful absorbing bands are centered around 1.6, 2.2, and 3.7 μm, with the longer wavelength bands having the greater absorption. These will be referred to collectively as near-infrared bands (also referred to as shortwave and midwave infrared bands). In each near-infrared band, droplet absorption increases with cloud droplet size over the expected size range. The greater the droplet absorption the less the cloud reflectance, all else being equal, and so near-infrared reflectance measurements contain information about droplet effective radius. However, these reflectances may also depend on optical thickness. Thin clouds provide little cumulative absorption to reflected photons because of the relatively small number of scatterings which can occur, and so reflectance is highly dependent on optical thickness. As a cloud becomes thicker, the near-infrared reflectance eventually reaches an asymptotic limit, potentially much less than unity, as absorption eliminates the possibility that deeply penetrating photons can survive the increasing number of scattering events required to return to cloud top. Beyond this limit, reflectance is constant with optical thickness, leaving only a droplet size dependence. The value of the asymptotic reflectance limit decreases with increasing absorption (or with droplet size for a given band) as does the corresponding optical thickness. The 3.7 μm band reflectance is therefore least dependent on cloud thickness, reaching the reflectance limit at about an optical thickness of 5. Simultaneous reflectance measurements in nonabsorbing and absorbing bands therefore contain the essential information required to infer both optical thickness and effective radius. A graphical summary of these concepts can be found in the plots of *Nakajima and King* [1990], *Rawlins and Foot* [1990], and *Platnick et al.* [2000].

Retrieval algorithms compare measured reflectances with calculated reflectances derived from homogeneous, plane-parallel cloud models. These modeled reflectances are usually in the form of libraries which span the expected range of optical thickness, droplet effective radius, and solar and viewing geometry. The retrieved optical thickness and effective radius corresponds to the library reflectances (from at least two bands) which are collectively closest, in some sense, to the measured reflectances. Therefore retrievals of real-world clouds give the parameters of a homogeneous cloud having nearly the same spectral reflectances as the measured cloud for the particular geometry. Various implementations of this basic approach with the 1.6 and 2.2 μm bands are described in the literature [*Twomey and Cocks*, 1989; *Nakajima and King*, 1990; *Rawlins and Foot*, 1990]. The 3.7 μm band size retrieval is complicated by cloud thermal emission which can be a significant part of the measured radiation. Since cloud emissivity will vary with droplet absorption, thermal emission is a function of temperature as well as droplet size. An algorithm must therefore search for the effective radius that gives an above-cloud intensity consistent with both solar reflectance and cloud emission. Satellite retrievals with this band include *Arking and Childs* [1985], *Platnick and Twomey* [1994], *Han et al.* [1994], and *Platnick and Valero* [1995]. It has also been demonstrated that there is size information in cloud emissivity at longer wavelengths [*Parol et al.*, 1991; *Ackerman et al.*, 1995].

A similar approach can be attempted for transmittance [*Rawlins and Foot*, 1990], though for several reasons, such a measurement (either bidirectional or flux) is much less dependent on effective radius than reflectance. First, transmittance as a function of optical thickness is always bounded by the same values regardless of wavelength or cloud microphysics (e.g., flux transmittance goes from unity in the absence of a cloud to zero for infinitely thick clouds). In these two thickness limits there is no possible cloud information in a transmittance

measurement. Second, at intermediate thicknesses the increase in forward scattering with droplet size tends to cancel the accompanying increase in droplet absorption, and once again, little microphysical information is available. However, for the same reasons, transmittance in any one of the spectral bands is capable of reasonably good optical thickness retrievals.

In the remaining sections we will discuss photon transport in reflectance, transmittance, and emittance problems. However, the emphasis will be on reflectance-based effective radius retrievals of stratus clouds. These plane-parallel-like clouds are most likely to be compatible with retrieval cloud models but may still have significant vertical inhomogeneities across the scales of photon transport. These inhomogeneities may lead to errors or biases in the retrieved cloud effective radius. Clearly, there are other potentially significant and more fundamental sources of retrieval error, such as uncertainties in the calculation of homogeneous cloud reflectances, instrument error, and atmospheric effects [e.g., *Han et al.*, 1994, 1995; *Platnick and Valero*, 1995]. There is also an unexplained tendency for size retrievals to be significantly larger than in situ measurements, i.e., anomalous absorption [*Twomey and Cocks*, 1989; *Nakajima et al.*, 1991]. It is within this overall context that effects of cloud inhomogeneities should also be examined. A better understanding of retrieval uncertainty is especially important given the interest in global droplet size climatologies [*King et al.*, 1992; *Han et al.*, 1994].

3. Vertical Cloud Structure

Cloud retrievals are based on homogeneous cloud models. However, it is known from both simple theoretical models and empirical data that cloud droplet sizes are likely to increase significantly with height in a nonprecipitating cloud. From theoretical considerations an adiabatic cloud profile has liquid water content increasing linearly with height over large thicknesses. Then, to the extent that droplet concentrations are found to be relatively constant with height, droplet sizes would also increase with height. A number of in situ measurements of cloud droplet size and/or liquid water content vertical profiles have been reported [*Slingo et al.*, 1982; *Noonkester*, 1984; *Nicholls and Leighton*, 1986; *Curry*, 1986 for arctic stratus; *Stephens and Platt*, 1987; *Gerber et al.*, 1994; *Garrett and Hobbs*, 1995]. As an example, Garrett and Hobbs measured effective radius increases at cloud top of about 50 and 100% relative to cloud base in two stratocumulus case studies near the Azores. It is difficult to obtain statistically meaningful profiles, which require sufficient sampling at all levels in the same cloud region, and so profile measurements often appear rather noisy. Nevertheless, most clouds appear to have liquid water content profiles that are subadiabatic to some extent, especially near cloud top [e.g., *Nicholls and Leighton*, 1986], therefore having less drastic size increases with height compared to an adiabatic cloud. Droplet size profiles sometimes have a nonlinearity suggestive of an adiabatic, or near-adiabatic, liquid water content profile. In other cases, droplet sizes seem to increase linearly with height. Several analytical models for droplet size profiles are derived momentarily.

Because of varying absorption, microphysical retrievals from the three near-infrared bands will sample different vertical portions of the cloud, and a given retrieval therefore represents the average radiative effect of the droplet size profile. A reflectance measurement in the 1.6 μm band is least affected by absorption and can contain information regarding droplet sizes in relatively deep layers of the cloud. The 2.2 and 3.7 μm bands have progressively more absorption, and the vertical sampling is more shallow. Clearly, a single effective radius for describing cloud radiative properties is rather ambiguous from the remote sensing standpoint, especially when using multiple near-infrared bands. Of course, the concept of a "correct" size retrieval is only meaningful in terms of the intended application (e.g., determination of liquid water path, broadband fluxes, influence of CCN).

3.1. Analytic Droplet Size Profiles

We wish to develop models of cloud droplet size profiles for use in assessing the impact of vertical structure on effective radius retrievals and the utility of vertical weighting functions discussed in the next section. The vertical structure will be given by simple analytic formulae derived from various prescribed physical constraints and not from cloud dynamic and microphysical models.

The following nomenclature is used: the vertical variable for the radiation problem is optical depth τ, measured from cloud top downward, while the term cloud optical thickness τ_c is used to indicate the overall optical depth down to cloud base. For example, we may refer to a level at an optical depth of 5, in a cloud with an optical thicknesses of 10. We therefore require a specification of effective radius as a function of optical depth for a given optical thickness, i.e., $r_e(\tau, \tau_c)$. In terms of geometrical height z, defined to increase from zero at cloud base to h at cloud top, optical depth at a wavelength λ is given by

$$\tau_\lambda(z) = \int_z^h dz' \int_0^\infty Q_{e_\lambda}(r)\pi r^2(z')n(r, z')\, dr$$

$$\approx \int_z^h 2\pi\overline{r^2(z')}N(z')\, dz', \qquad (1)$$

where the extinction efficiency $Q_{e_\lambda}(r)$ is ~2 for cloud droplet size particles at the wavelengths of interest, and $N(z)\, dz$ is the total droplet number per unit area in the differential layer between z and $z + dz$.

Consider an adiabatic cloud. Liquid water content (LWC) in a saturated adiabatic process increases linearly with geometric height for lower clouds and over extended thicknesses. Therefore we can write liquid water at the height z as

$$\mathrm{LWC}(z) = C\int_0^\infty r^3(z)n(r, z)\, dr = C\overline{r^3(z)}N(z) \sim z, \qquad (2)$$

where $C = 4\pi\rho_l/3$, and ρ_l is the density of liquid water. Ignoring differences among the area-weighted, volume-weighted, and effective radius [*Martin et al.*, 1994], (2) becomes $r_e^3(z)N(z) = b_0 + b_1 z/h$, where b_0 and b_1 are constants. Assuming N is constant with height, $r_e(z) \propto (b_0 + b_1 z/h)^{1/3}$. A curvature of this type (second derivative less than zero) is often seen in measured profiles [e.g., *Stephens and Platt*, 1987]. Differentiation yields $dz \propto Nr_e^2(z)\, dr_e$. Substitution into the second form of (1) and integrating over r_e from $r_e(z)$ to the cloud-top effective radius, r_{top}, gives $\tau \propto (r_{\mathrm{top}}^5 - r_e^5(z))$. The size profile can now be expressed in terms of optical depth instead of geometric height. Rearranging gives $r_e(\tau, \tau_c) = (a_0 - a_1\tau/\tau_c)^{1/5}$ where the constants $a_0 = r_{\mathrm{top}}^5$ and $a_1 = r_{\mathrm{top}}^5 - r_{\mathrm{base}}^5$ are determined from prescribed boundary conditions on droplet size, with r_{base} as the cloud base effective

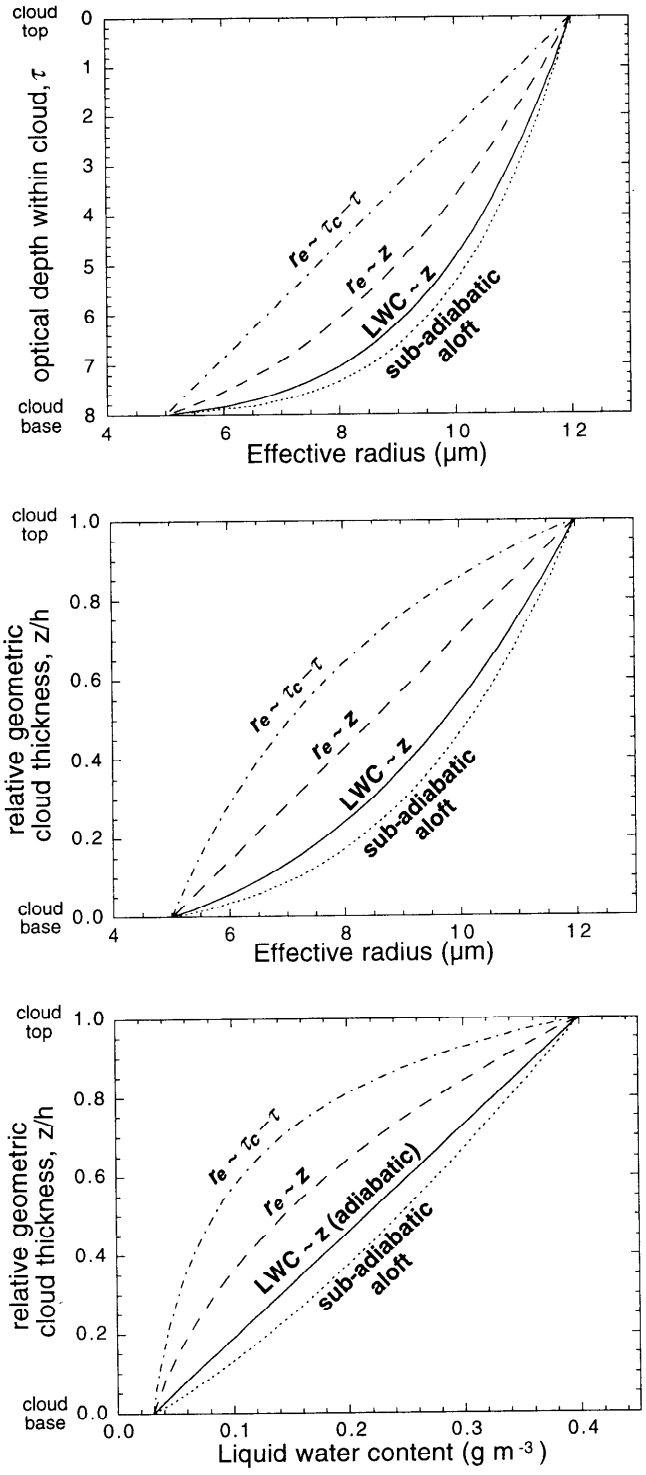

Figure 1. Example of the four analytic models for the vertical profile of effective radius r_e given in Table 1 for the same prescribed boundary conditions (total cloud optical thickness τ_c is 8 and effective radius is 5 and 12 μm at cloud base and top, respectively). The top plot shows effective radius as a function of optical depth τ. The bottom two plots show the corresponding profile of r_e and cloud liquid water content (LWC) as a function of geometric height z, where h is the total thickness. The constraints used in deriving the profiles are indicated along the side of each curve. Note that for an otherwise identical cloud process, cloud top r_e and LWC would be smaller for the subadiabatic profile (shown for $x = 0.75$).

radius. Though cloud base should be strictly defined as the level where liquid water content and droplet size are zero, the location of cloud base from in situ measurements is ambiguous due to sampling difficulties, uncertainty associated with the measurement of small liquid water content and droplet sizes, and the rapid increase in droplet size over relatively small vertical scales. In addition, these thin bottom layers with small droplet sizes make the least contribution to cloud optical thickness. For these reasons, a well-defined cloud base with a nonzero boundary condition is used. An example of an adiabatic droplet size profile as a function of both optical depth and height is shown in Figure 1 for $\tau_c = 8$, $r_{\text{base}} = 5$ μm, and $r_{\text{top}} = 12$ μm. Droplet sizes are seen to quickly increase with height from cloud base. The linear liquid water content profile is also shown. Boundary conditions are consistent with a droplet concentration of about 60 cm^{-3}. Analytic formulae for the adiabatic cloud model are summarized in Table 1 (profile B).

A subadiabatic liquid water content profile, having adiabatic liquid water near cloud base but with increasing entrainment, or drying, toward cloud top, can be specified with the power law $(c_0 + c_1 z/h)^x$, where $0 < x < 1$ and c_0, c_1 are again constants determined from the boundary conditions. Equations for the droplet size profiles are given in Table 1 (profile A). An example with $x = 0.75$ is shown in Figure 1 as the subadiabatic aloft profile. The reduction in cloud-top liquid water results in less change in droplet size in the upper portions of the cloud. Note that all curves in Figure 1 have identically prescribed microphysical boundary conditions. For clouds forming in otherwise identical meteorological conditions, liquid water content and droplet size in the subadiabatic cloud model should, of course, be smaller at upper levels. Prescribing equivalent liquid water content in the lower parts of the cloud, the subadiabatic model with $x = 0.75$ gives a cloud-top liquid water content about 60% less than the comparable adiabatic cloud.

Measured droplet size profiles often appear to be linear with height [e.g., *Stephens and Platt*, 1987]. It can be shown that $r_e(z) \sim z$ implies LWC $\sim z^3$ and $r_e(\tau, \tau_c) = (a_0 - a_1\tau/\tau_c)^{1/3}$, an analytic form similar to the adiabatic and subadiabatic profiles (profile C). For the same prescribed boundary conditions, this profile gives subadiabatic liquid water content at midlevels (e.g., the occurrence of a drying process in middle layers) and droplet sizes decreasing more rapidly with depth in the upper part of the cloud than for the adiabatic profile (see Figure 1). Though this size profile is recognizable in measurements, the accompanying liquid water profile is not obvious in the in situ profiles previously cited and might only be applicable to multilayer or decoupled cloud layers. A profile with droplet size decreasing even more rapidly with depth in the upper part of the cloud can be found by simply specifying effective radius to be linear in optical depth; that is, $r_e(\tau, \tau_c) = a_0 - a_1\tau/\tau_c$ (profile D).

Table 1 and Figure 1 summarize the four analytic droplet size profiles discussed. Consider a reflectance-based retrieval. All bands sample the upper portions of the cloud more readily than lower parts, even for a band with no absorption (e.g., in the visible). Regardless of the assumed profile, droplet size retrievals with each of the near-infrared bands will differ due to increasing droplet absorption with band wavelength. It is the profile in the upper parts of the cloud which has the most influence on retrieval size and band differences. For the same prescribed boundary conditions, a profile having small values

Table 1. Analytic Models for the Vertical Structure of Effective Radius r_e and Liquid Water Content (LWC) Versus Geometric Cloud Height z and Optical Depth τ

LWC (z)	$r_e(z)$	$r_e(\tau)$	a_0	a_1
		Vertical Structure		
$\left(c_0 + c_1 \frac{z}{h}\right)^x$	$\left(b_0 + b_1 \frac{z}{h}\right)^{x/3}$	$\left(a_0 - a_1 \frac{\tau}{\tau_c}\right)^{x/2x+3}$	$r_{top}^{2x+3/x}$	$r_{top}^{2x+3/x} - r_{base}^{2x+3/x}$

Profile	Constraint	x	Physical Implication
A	subadiabatic aloft	$0 < x < 1$	increasing entrainment/drying toward cloud top
B	LWC (z) $\sim z$	1	adiabatic
C	$r_e(z) \sim z$	3	subadiabatic at midlevels
D	$r_e(\tau) \sim \tau_c - \tau$	−3	subadiabatic at midlevels (useful test of weighting formulations)

The following convention is used: z increases from $z = 0$ at cloud base to $z = h$ at cloud top; optical depth increases toward cloud base with $\tau = 0$ at cloud top; τ_c is the total cloud optical thickness. The constants a_0, a_1 are found from the optical thickness and the prescribed boundary conditions for droplet size at cloud top and base, r_{top} and r_{base}, respectively. Other constants (b, c) can be determined in a similar manner.

for $|dr_e/d\tau|$ in upper portions of the cloud will have sizes more nearly constant with optical depth, implying larger retrievals and smaller retrieval differences among the bands. Therefore all near-infrared bands will infer the largest droplet size for the subadiabatic aloft profile (see top plot of Figure 1); retrievals for the adiabatic profile would not be much less. Size retrievals would be smallest for profile *D* which has the largest values of $|dr_e/d\tau|$ at upper levels. Near-infrared retrieval differences would also be greatest for this profile, making it helpful for assessing the capability of weighting functions.

Four example test clouds, based on the adiabatic and linear profiles (*B* and *D* in Table 1), are used in much of the subsequent analyses. These two profiles provide a useful range in $|dr_e/d\tau|$ at upper levels. Table 2 summarizes the four test clouds for both profiles. Optical thicknesses range from a relatively small $\tau_c = 5$ to a moderately thick $\tau_c = 15$. Clouds with thicknesses less than $\tau_c = 5$ will not have a significant vertical signature. Clouds up to $\tau_c = 15$ span the asymptotic limit for 2.2 and 3.7 μm band reflectances (see section 2); that is, lower layers will be inconsequential in these bands for thicker clouds. The thickest cloud is assigned the smaller droplet sizes (less absorption) to allow lower layers some influence on reflectance. The range of radii from cloud top to base is somewhat larger than typical in situ measurements but still realistic. For numerical purposes the test clouds are built up from individual homogeneous layers with optical thicknesses of 0.25 and integer values of effective radii. Liquid water path is determined from the summation of the product of layer optical thickness and effective radius (equations (1) and (2) approximate the water path in layer i as $2r_{ei}\Delta\tau_i/3$, in units of g m^{-2} for r_e in micrometers). Other microphysical quantities such as liquid water content (LWC) and droplet concentration N cannot be uniquely determined from specification of optical thickness and effective radius alone. Liquid water content requires knowledge of N, and only the product Nh is specified (equation (1)). Table 2 gives values of N and LWC for a fixed geometric thickness of 0.3 km (recall N is constant with height in the models). The small values of N, representative of pristine conditions, are a consequence of the relatively large prescribed cloud-top effective radii. The adiabatic profile has the more reasonable liquid water content, whereas the other profile is wetter due to larger droplet concentrations. Model results and conclusions are discussed at the end of the next section. Results from the other two analytic profiles were also examined. The $r_e \sim z$ profile (*C*) is used in many of the weighting function plots.

Table 2. Two Analytic Profiles for Cloud Droplet Effective Radius As a Function of Optical Depth (See Table 1) and Resulting Cloud Liquid Water Path (LWP), Liquid Water Content (LWC), Droplet Number Concentration (N, Assumed Constant With Height), and Geometrical Thickness (h)

Cloud Specifications		Vertical Structure							
		Profile *D*				Profile *B* (Adiabatic)			
τ_c	r_e Cloud Base-Top, μm	LWP, g m^{-2}	Nh, cm^{-3} km	N for $h = 0.3$ km, cm^{-3}	LWC of Base, Top Layer for $h = 0.3$ km, g m^{-3}	LWP, g m^{-2}	Nh, cm^{-3} km	N for $h = 0.3$ km, cm^{-3}	LWC of Base, Top Layer for $h = 0.3$ km, g m^{-3}
15	4–10	75	60.6	202	0.05, 0.85	89	37.0	123	0.06, 0.52
10	6–15	74	17.8	59	0.05, 0.84	88	11.1	37	0.05, 0.52
8	5–12	48	21.3	71	0.04, 0.51	57	13.8	46	0.04, 0.33
5	8–12	35	8.2	27	0.06, 0.20	37	7.5	25	0.05, 0.18

Example microphysics are given for $h = 0.3$ km. Optical thickness is scaled to a wavelength-independent extinction efficiency of $Q_e = 2.0$. Clouds are built up from homogeneous layers with scaled optical thicknesses of 0.25 and integer effective radii as described in the text.

4. Multiple-Scattering Weighting Functions

Two immediate questions come to mind. First, to what extent do the three near-infrared bands infer different effective radii for realistic size profiles? Second, do measurements in the near-infrared bands contain information sufficient to infer the size profile? That is, can an inversion technique be devised.

One approach to these questions is to make repeated forward calculations of cloud reflectance (or transmittance, emittance) with various vertical profiles and use the results as input to a retrievals code. However, the exercise would provide limited insight since information is unavailable on the contribution of individual layers to the retrieval result. The lack of layer information would also make it difficult to assess the possibility of implementing an inversion for the size profile. A more useful approach is to understand the radiative contribution that various layers impart to the overall size determination. For a single-scattering problem this is achieved by couching the problem in terms of vertical weighting functions describing the intensity at a boundary in terms of the cumulative contribution of individual layers. A common example is an infrared sounding technique, where the weighting function at some wavelength is derived from the net transmittance between an emitting layer and the top or bottom of the atmosphere. In the solar region, backscattered ultraviolet measurements infer stratospheric ozone profiles with weighting functions given by ozone path absorption. The single-scattering condition provides a one-to-one correspondence between the emitted or scattered radiation from some level and the measured signal. In the case of the cloud problem, multiple scattering destroys this correspondence as radiation may scatter in many layers. However, this does not exclude the possibility of useful, though approximate, vertical weighting functions for multiple-scattering problems.

For the retrieval of cloud droplet sizes we seek a weighting function w, defined such that the retrieved effective radius r_e^*, determined from near-infrared solar reflection or transmission measurements of a cloud with known optical thickness τ_c, can be estimated from

$$r_{e\lambda}^* = \int_0^{\tau_c} r_e(\tau) w_\lambda(\tau, \tau_c)\, d\tau. \tag{3}$$

The dependence of the weighting function on $r_e(\tau)$ and solar and viewing geometry is not shown explicitly; that is, $w_\lambda = w_\lambda(\tau, \tau_c, \mu, \mu_0, r_e(\tau))$, where μ_0 and μ are the cosine of the solar and viewing angles, respectively. The more explicit notation will be used only when needed. Note that the weighting function is normalized in this definition, i.e., (3) must give $r_e^* = r_e$ for a droplet size profile that is constant with height. Both r_e^* and w are shown as wavelength or band dependent, giving a set of inversion-like formula for $r_e(\tau)$. The ability to infer $r_e(\tau)$ ultimately depends on the relative orthogonality of the near-infrared weighting functions as discussed in section 6.

The weighting function needs to capture the multiple-scattering nature of the problem. Weightings based on single-scattering properties, such as layer extinction or single-scattering albedo will not, in general, be sufficient [*McFarquhar and Heymsfield*, 1998]. Several possibilities for an appropriate weighting function exist. We begin with a simple weighting for reflected radiation.

4.1. Weighting by Maximum Vertical Photon Penetration

A weighting proportional to the maximum vertical penetration obtained by photons will capture some aspect of the multiple-scattering process for reflected radiation. Such a weighting could, of course, be found from a Monte Carlo calculation where the total fraction of reflected photons penetrating to each layer can be determined. However, such a method is computationally intensive. A faster and more efficient mean of calculating this weighting is through superposition principles.

Consider the bidirectional reflectance $R(\tau_c)$, from a cloud with optical thickness τ_c, overlying a black surface. The addition of a differential layer $d\tau$ to the base of the cloud results in a reflectance increase of $dR = R(\tau_c + d\tau) - R(\tau_c)$. By definition, dR represents the part of the total reflected signal $R(\tau_c + d\tau)$ contributed by photons that penetrate only as deep as the $\tau_c + d\tau$ layer. Photons penetrating deeper would be absorbed by the black surface, while photons having all scatterings above the τ_c level do not contribute to dR. Therefore the ratio $dR/R(\tau_c + d\tau) \approx dR/R(\tau_c)$ must represent the fraction of all reflected photons that penetrate to a maximum depth between τ_c and $\tau_c + d\tau$. This must also hold true for arbitrary layers within a cloud; that is, $(R(\tau + d\tau) - R(\tau))/R(\tau_c)$ gives the fraction of all reflected photons that penetrate to a maximum depth between τ and $\tau + d\tau$, in a cloud of optical thickness τ_c, where $R(\tau)$ is the reflectance from the portion of the cloud above the level τ (i.e., calculated with lower layers absent). A normalized weighting compatible with (3) is therefore

$$w_m(\tau, \tau_c) = \frac{\dfrac{dR(\tau)}{d\tau}}{R(\tau_c)}, \tag{4}$$

with the subscript m signifying a maximum penetration weighting and the wavelength-dependence understood. It should be noted that the derivative is calculated for a $d\tau$ layer added to the base of the cloud, not the top, an important distinction when cloud microphysics varies with height.

The interpretation of w_m as a weighting proportional to maximum photon penetration is valid for a black surface. Accounting for surface-reflected photons is at odds with the weighting definition since all such photons will have passed through the deepest possible cloud level, i.e., cloud base, at least once. The extent to which a known surface reflectance will modify the inference of effective radius r_e^* for a vertically inhomogeneous cloud will be discussed later. If the difference between the retrieval with and without a typical surface reflectance is negligible, then (4) is still directly applicable. Otherwise, a modification to the weighting is required (equation (3)).

Calculations are made using the adding/doubling or superposition technique of *Twomey et al.* [1966]. Only the fundamental, or azimuthally averaged reflectances, are presented, which should be sufficient for the multiple-scattering problems being considered. Because of reciprocity in bidirectional reflectance [*Chandrasekhar*, 1960, p. 172], an exchange of solar and viewing directions does not change the weighting function; that is, $w_m(\tau, \tau_c, \mu, \mu_0) = w_m(\tau, \tau_c, \mu_0, \mu)$. A maximum penetration weighting for a reflected flux (albedo) measurement can be calculated in a similar manner; bidirectional reflectance in (4) is simply replaced by the albedo. An example of the weighting function is plotted in Figure 2 for profile C. Details of the cloud model are given in the figure caption. The shape of the weighting function will be discussed shortly. Ex-

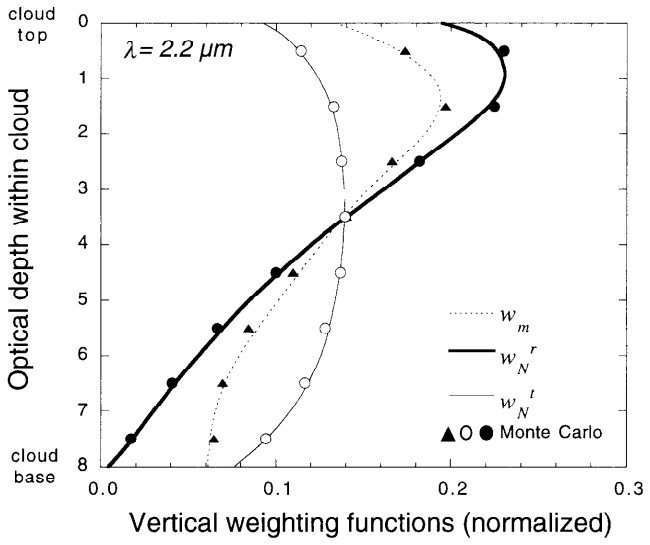

Figure 2. Two proposed normalized vertical weighting functions, w_m (proportional to maximum photon penetration) and w_N (proportional to number of photon scatterings), for a 2.2 μm spectral channel, using both superposition formulae (lines) and Monte Carlo calculations (symbols). Calculated for the cloud of Figure 1 using profile C in Table 1, cosine of solar zenith and viewing angles of $\mu_0 = 0.65$ and $\mu = 0.85$, respectively, and an azimuthal average. Plots of the scattering number weighting function include weightings for both reflected and transmitted radiation, w_N^r and w_N^t, respectively.

cellent agreement with Monte Carlo calculations, also shown in the plot, confirms the interpretation of (4) and verifies its numerical implementation.

4.2. Weighting by the Average Number of Photon Scatterings

A weighting proportional to the average number of photon scatterings in individual cloud layers would seem more capable of accounting for the effect of multiple scattering on retrievals. For example, consider a reflectance-based retrieval. In a Monte Carlo calculation, such a weighting can be found from the total number of scatterings encountered by reflected photons in each layer. The normalization is then the total number of reflectance scatterings. Dividing the number of scatterings in each layer by the total number of reflected photons gives an alternative expression for the weighting. Now the normalization becomes the average number of scatterings for all reflected photons, and the weighting is proportional to the average number of reflectance scatterings in each layer. For example, a layer average of 0.5 can be interpreted as meaning that on average, half of all reflected photons had a scattering in that layer. This fraction will be much less than 1 for thin layers and can be greater than 1 if the layer is thick enough to generate multiple scattering.

Though this weighting is more involved than w_m, where only the deepest scattering layer encountered by a photon was considered, it remains to be seen whether it provides a better weighting in the sense of (3). However, unlike w_m, a weighting based on layer scattering can be defined for transmittance as well as reflectance. We designate this weighting by w_N^r, where the subscript N signifies a number of scatterings weighting and the superscript r refers to a reflectance weighting (superscript t will refer to a transmittance weighting). Monte Carlo calculations are computationally intensive and would limit the utility of the weighting. As before, a much more efficient means of calculating this weighting is also available through superposition principles and is described in detail by *Platnick* [2000b]. Once again, all calculations are made using the adding/doubling matrix formulation of *Twomey* [1966]. As with the maximum penetration weighting, there is also reciprocity upon exchange of solar and viewing directions for the bidirectional form of this weighting.

Examples of a reflectance and transmittance weighting for a 2.2 μm channel are shown in Figure 2. Calculations are for $\tau_c = 8$ and effective radius profile $C(r_e \sim z)$ with cloud base and top effective radii of 5 and 12 μm, respectively. Other details are given in the caption. Both superposition and Monte Carlo calculations are shown. The agreement is excellent, establishing the use of superposition formulae in calculating these plane-parallel scattering statistics. The average number of scatterings also agree with Monte Carlo calculations for both reflected and transmitted photons at all optical thicknesses of interest [*Platnick*, 2000b]. The figure also shows the maximum penetration weighting for reflectance w_m. In both cases the upper part of the cloud is weighted more heavily then lower portions as expected, with w_N^r being the more extreme. The transmittance weighting is relatively symmetric with optical depth, showing a broad maximum throughout the middle layers of the cloud. Figure 3 shows the weighting functions for three different cloud optical thicknesses, with the same microphysics and geometry of Figure 2. The decrease in w_m toward cloud top is due to an initial increase in the derivative $dR/d\tau$ (equation (4)) for thin clouds. Note that at any given level, $dR/d\tau$ will increase if effective radius decreases (a result of both decreasing asymmetry parameter and droplet absorption at smaller radii). This explains the slight increase in w_m near cloud base for the thinnest cloud example where smaller effective radii in the lowest layer are contributing incrementally more to the overall reflectance than adjacent layers.

5. Retrieval Examples for Vertically Inhomogeneous Clouds

The accuracy of the proposed weightings in estimating retrieved effective radii via (3) was tested on the two profiles described in Table 2. Four clouds, each with different optical thicknesses and effective radius boundary conditions, are considered for each profile, as discussed in section 3.1. As mentioned, the model clouds were built up from thin homogeneous cloud layers of optical thickness 0.25. Each layer was assigned an effective radius equal to the integer value closest to the profile-specified size at the depth corresponding to the layer midpoint. Reflectances in the various bands were calculated for the model cloud using the superposition/adding techniques already discussed. These reflectances then served as measurement input to a retrieval code which determined effective radius by matching the model cloud reflectance with entries in a homogeneous cloud reflectance library spanning the expected range of retrieved radii and optical thickness (see section 2 for more detail). Comparisons between weighting-derived size estimates and the retrieval code are made for each of the three near-infrared bands.

In the usual algorithm implementation, an absorbing and nonabsorbing band are used to retrieve effective radius and optical thickness. For the vertically inhomogeneous cloud, this can lead to slight differences between the retrieved and the actual optical thickness. The optical thickness error may then

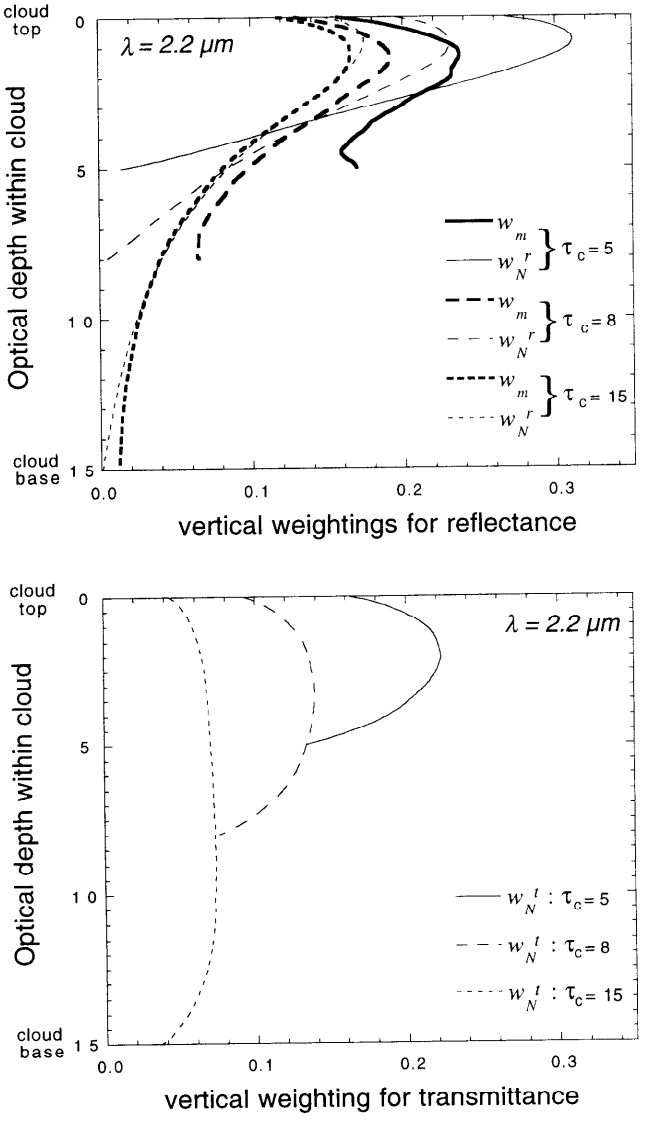

Figure 3. Dependence of the normalized vertical weighting functions on cloud optical thickness for reflected (top plot) and transmitted (bottom) radiation, for a 2.2 μm spectral channel. Calculated for the same droplet size profile, microphysical boundary conditions, and geometry of Figure 2.

affect size retrievals. This is most pronounced when using the less absorbing near-infrared bands in conjunction with thin clouds. To the extent that the weighting function estimate from (3) implicitly assumes that optical thickness is known, it is useful to isolate the size retrieval from its optical thickness dependence. So for consistency, retrievals in the following comparisons are made with the optical thickness specified. However, letting the optical thickness be a variable during the retrievals only had minor impact, typically modifying retrieved effective radii by less than 0.2 μm for the 1.6 and 2.2 μm bands; no differences are found in 3.7 μm size retrievals because of the band's greater absorption. The 3.7 μm band results use the reflectance signal only, i.e., removal of cloud emission is assumed to occur without error. Further, all retrievals are made in the absence of an atmosphere and with a black surface.

5.1. Tests of the Weighting Functions

The comparisons are shown in Table 3a for a bidirectional reflectance measurement with cosines of the solar and viewing zenith angles of 0.65 and 0.85, respectively. The first column under each profile gives the effective radius from the retrieval code. The second and third columns estimate the retrieval with (3) using weightings w_m and w_N^r, respectively. Results are shown for each of the three near-infrared bands.

Several observations can be made. First, since effective radius was specified to increase with height, retrieved sizes increase with band wavelength (i.e., water absorption). Second, differences between 1.6 and 2.2 μm retrievals are always less than between those bands and the 3.7 μm band retrieval. The magnitude of the size difference depends on cloud thickness and droplet size profile. Differences between 1.6 and 3.7 μm band size retrievals vary from 0.8 to 1.5 μm for the adiabatic profile. The 1.6 and 2.2 μm band retrieval differences are smaller, ranging from 0.3 to 0.6 μm. As expected, for otherwise identical clouds, retrievals for profile D are always less than for the adiabatic profile, and differences among the near-infrared retrievals are larger by more than several micrometers. Conversely, the subadiabatic aloft profile (A) results in slightly larger retrievals in all bands compared with the adiabatic cloud model, and differences between the bands are somewhat smaller (not shown).

Both weightings do a good job in approximating the retrieved radius and are practically equivalent in the 3.7 μm band. However, the maximum penetration weighting, w_m, gives the best retrieval estimate for all bands over a wide range of cloud thicknesses and droplet sizes. The average number of scatterings weighting w_N^r tends to overestimate the retrieved size more than w_m. This is somewhat surprising given the higher-order scattering information contained in the weighting. In an attempt to reduce the size estimate, various modifications to the w_N^r weighting were considered, including one proportional $N_i \varpi_{0i}^{Ni}$, where ϖ_{0i} is the layer single-scattering albedo. This modification typically reduced the size estimates by only a tenth of a micrometer, leaving the w_m estimate as the preferred weighting. Fortunately, the w_m weighting also has the advantage of being the simplest to calculate. For all cloud models in Table 3a, differences between w_m size estimates and retrievals for the adiabatic profile are within 0.3 μm for the 1.6 μm band and within 0.1 μm for the 2.2 and 3.7 μm bands. These differences are small compared with estimates of size uncertainty based on homogeneous cloud retrievals [*Platnick and Valero*, 1995]. The subadiabatic aloft profile results in slightly smaller differences. For profile D, size differences are within 0.9, 0.2, and 0.2 μm for the 1.6, 2.2, and 3.7 μm bands, respectively. With the exception of the 1.6 μm band retrieval estimate, agreement is still excellent.

As another test of the weightings, consider clouds with effective radii decreasing with height. While such a profile might be physically realizable in clouds containing drizzle, the current interest is mainly in checking the accuracy of the weightings when the more absorbing layers are located toward cloud base. This effectively increases photon penetration compared with an otherwise similar cloud having the larger radii at the top. Comparisons using the models in Table 3a were repeated but with the size profiles reversed from top to base (described by the identical profiles of Table 1, but with the original boundary conditions r_{base} and r_{top} switched). The adiabatic profile now decreases relatively slowly from cloud base upward, with a

Table 3a. Comparison of Reflectance-Inferred Effective Radius Retrievals With Estimates Obtained From Vertical Weightings w_m and w_N^r Using Equation (3) Versus Spectral Band

Cloud Specifications			Vertical Structure					
			Profile *D*			Profile *B* (Adiabatic)		
τ_c	λ, μm	r_e Cloud Base-Top, μm	r_e^* Retrieval, μm	r_e^* w_m Estimate, μm	r_e^* w_N^r Estimate, μm	r_e^* Retrieval, μm	r_e^* w_m Estimate, μm	r_e^* w_N^r Estimate, μm
15	1.6	4–10	7.3	7.9	8.1	8.8	9.1	9.3
	2.2		8.1	8.3	8.4	9.3	9.3	9.4
	3.7		9.4	9.3	9.3	9.9	9.9	9.9
10	1.6	6–15	10.8	11.3	12.0	13.0	13.2	13.7
	2.2		11.8	11.7	12.2	13.6	13.5	13.9
	3.7		13.4	13.3	13.3	14.5	14.4	14.5
8	1.6	5–12	8.0	8.9	9.6	10.2	10.5	10.9
	2.2		9.1	9.1	9.7	10.7	10.6	11.0
	3.7		10.5	10.3	10.4	11.4	11.4	11.4
5	1.6	8–12	10.0	10.2	10.6	10.4	10.6	11.0
	2.2		10.3	10.3	10.7	10.7	10.7	11.0
	3.7		10.9	10.8	11.0	11.2	11.1	11.3

Retrievals give the droplet size of a homogeneous cloud with bidirectional reflectance equivalent to that of the vertically structured cloud. Calculations are for horizontally homogeneous plane-parallel cloud layers with effective radii increasing toward cloud top as described by the two analytic profiles in Table 2. The cloud optical thickness τ_c is assumed to be known exactly when determining both retrievals and weighting-derived estimates. Calculations are for cosine of the solar and viewing zenith angles of $\mu_0 = 0.65$, $\mu = 0.85$, respectively, an azimuthal average, and a black surface at all wavelengths.

rapid decrease near cloud top. Results are shown in Table 3b, where the w_m size estimate is now larger than the w_N^r estimate. Again, the w_m weighting estimates compare best with the retrievals, with overall differences similar to the previous results.

A further test of the w_m weighting can be made with two separate cloud layers, such as a midlevel cloud overlying a lower status deck, each having significantly different droplet sizes. Ignoring absorption and scattering in the medium between the clouds, the two layers can be modeled as a single contiguous cloud with a discontinuity in the droplet size profile. The discontinuity provides a more severe test of the weighting function, at least for bands where a significant part of the weighting is from the lower cloud layer. Consider two homogeneous clouds. Let R_1 be the reflectance in some band for the upper cloud alone and R_c the net reflectance resulting from the superposition of both clouds. Then from (4) the net integrated weighting for the upper and lower cloud layers is R_1/R_c and $(R_c - R_1)/R_c = 1 - R_1/R_c$, respectively. Applying (3) therefore gives a weighting-inferred effective radius estimate of $r_e^* = r_{e_1}(R_1/R_c) + r_{e_2}(1 - R_1/R_c)$, where r_{e_1} and r_{e_2} are the effective radii in the upper and lower clouds, respectively. As an example, let $r_{e_1} = 10$ μm, $r_{e_2} = 5$ μm, $\tau_1 = \tau_2 = 5$ (i.e., $\tau_c = 10$), $\mu = 0.85$, and $\mu_0 = 0.65$. The net weighting for the upper cloud is found to be 0.62, 0.68, and 0.92 for the 1.6, 2.2, and 3.7 μm bands, respectively, giving size estimates of 8.1, 8.4, and 9.6 μm, respectively. Estimates from the two longer wavelength bands are found to be within 0.2 μm of the actual retrievals (same analysis as Tables 3a and 3b), whereas the 1.6 μm size estimate is about 0.8 μm larger. As in Tables 3a and 3b, the 1.6 μm band weighting estimate tends to differ most from the retrieval. This is due to the band's relatively weak droplet absorption and hence limited size information for clouds much thinner than that corresponding to the asymptotic reflectance limit.

Table 3b. Same as Table 3a but for Plane-Parallel Cloud Layers With Effective Radii Decreasing Toward Cloud Top

Cloud Specifications			Vertical Structure					
			Profile *D*			Profile *B* (Adiabatic)		
τ_c	λ, μm	r_e Cloud Base-Top, μm	r_e^* Retrieval, μm	r_e^* w_m Estimate, μm	r_e^* w_N^r Estimate, μm	r_e^* Retrieval, μm	r_e^* w_m Estimate, μm	r_e^* w_N^r Estimate, μm
15	1.6	10–4	6.0	5.7	5.6	4.5	4.3	4.2
	2.2		5.6	5.4	5.3	4.2	4.2	4.2
	3.7		4.8	4.7	4.6	4.0	4.0	4.0
10	1.6	15–6	9.2	9.2	8.7	6.9	6.8	6.5
	2.2		8.6	8.7	8.4	6.6	6.6	6.4
	3.7		7.5	7.4	7.3	6.2	6.2	6.1
8	1.6	12–5	7.5	7.7	7.2	5.8	5.7	5.4
	2.2		7.2	7.3	7.0	5.6	5.5	5.4
	3.7		6.5	6.4	6.2	5.2	5.2	5.2
5	1.6	12–8	9.8	9.9	9.5	9.2	9.1	8.7
	2.2		9.7	9.8	9.5	8.9	9.0	8.7
	3.7		9.2	9.2	9.1	8.5	8.5	8.4

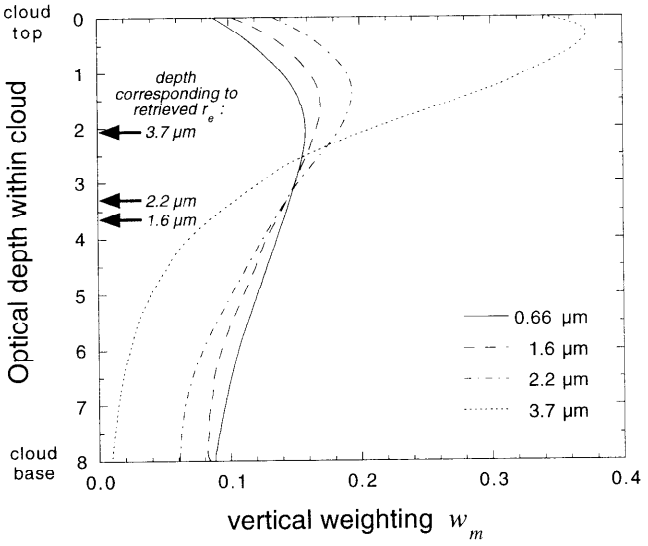

Figure 4. Normalized vertical weighting w_m for bidirectional reflectance, for visible and near-infrared cloud remote sensing channels, calculated using the superposition formulae discussed in the text, and the cloud described in Figure 2. The cloud optical depth corresponding to the retrieved radii for each near-infrared channel is also indicated.

We conclude that w_m provides an accurate, and apparently robust, weighting for use in (3). Further plots of this weighting are shown in Figure 4 for visible and near-infrared bands and the cloud described in Figure 2. The optical depth corresponding to the weighting-derived retrieved size is indicated in the plot.

5.2. Angular Dependencies

For the same cloud and solar zenith angle of Figure 4, Figure 5a shows the weighting dependence on viewing angle for each near-infrared band ($0.45 \leq \mu \leq 0.95$). The weighting for albedo is also shown. It is clear that larger viewing angles correspond to an increase in the upper cloud weighting. Retrieved sizes will therefore vary with both solar and viewing angles for vertically inhomogeneous clouds. Table 4 gives the retrieved effective radius in each band as a function of viewing angle for the adiabatic profile. Retrievals change by about 1 μm in the shorter wavelength bands for $0.15 \leq \mu \leq 0.95$. The optical depth corresponding to the retrieved size is also given in the table along with the corresponding relative geometric depth $1 - z/h$ (z is height from cloud base, h is total cloud geometric thickness). These depths are the level at which an in situ aircraft would have to fly to measure droplet sizes equivalent to the retrievals. The corresponding relative optical depth τ/τ_c ranges from less than 0.1 for the 3.7 μm band at $\mu = 0.25$ to over 0.5 for the 1.6 μm band at a nadir view; similarly, the relative geometric depth ranges from 0.05 to 0.4, respectively. Exchanging solar and viewing directions results in identical weightings, size estimates, and retrievals due to reciprocity in bidirectional reflectance as discussed previously. So the results of Figure 5a and Table 4 are also valid for $\mu = 0.65$ and μ_0 varying.

Two points can be made. First, aircraft microphysical sampling at a single cloud level may provide misleading validation results. Consider the adiabatic cloud example of Table 4 for $\mu = 0.85$. An aircraft flying in cloud, at an altitude equal to one third of the cloud geometric thickness, would measure an effective radius equivalent to the 2.2 μm band retrieval of 10.6 μm, similarly for the 1.6 μm band retrieval (10.5 μm). However, the 3.7 μm band retrieval would be 11.4 μm, or almost 1

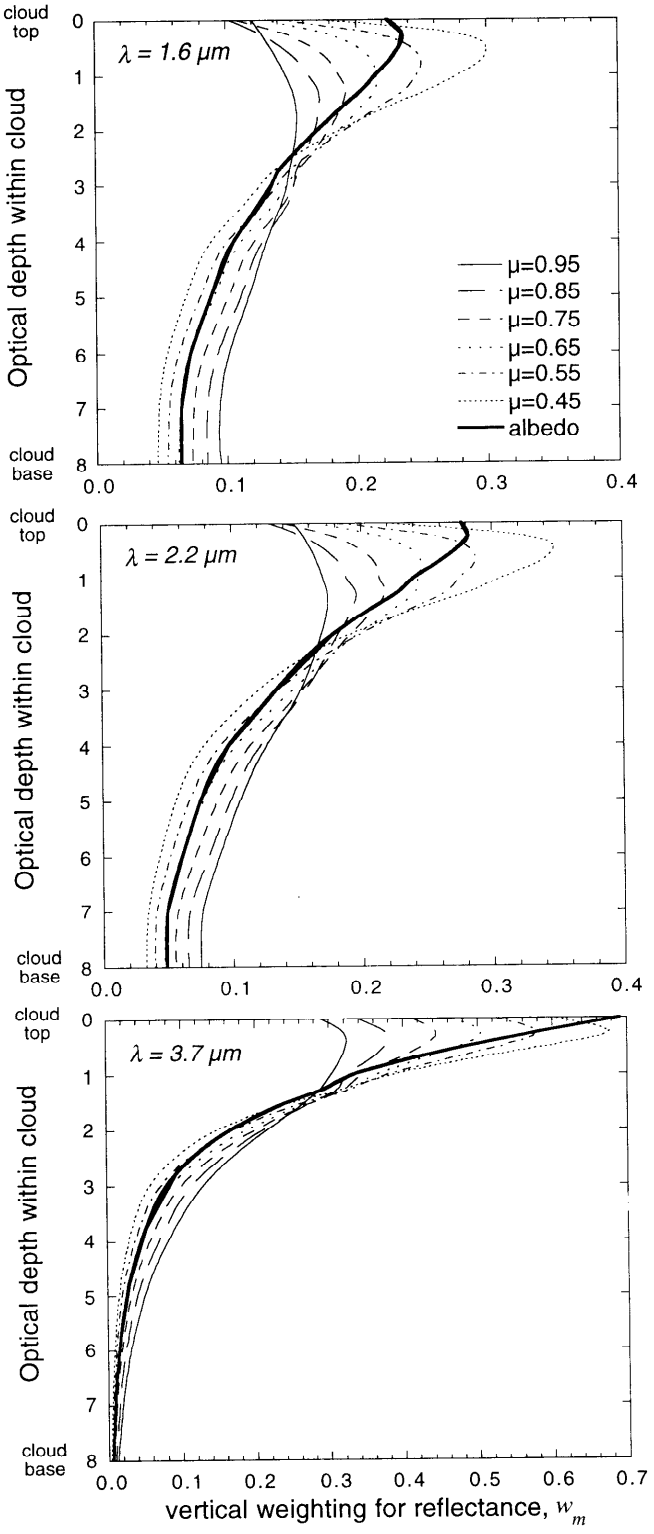

Figure 5a. Dependence of the normalized bidirectional reflectance weighting w_m on the cosine of the viewing angle μ for three near-infrared channels, and the cloud described in Figure 2. The weighting for reflected flux, or albedo, is also shown.

Table 4. Weighting-Derived Effective Radius Retrievals Versus Spectral Band and Cosine of the Viewing Zenith Angle, μ

Viewing Zenith Angle μ	1.6 μm			2.2 μm			3.7 μm		
	r_e^* w_m Estimate, μm	τ Corresponding to r_e^*	$1 - z/h$ Corresponding to r_e^*	r_e^* w_m Estimate, μm	τ Corresponding to r_e^*	$1 - z/h$ Corresponding to r_e^*	r_e^* w_m Estimate, μm	τ Corresponding to r_e^*	$1 - z/h$ Corresponding to r_e^*
0.95	10.4	4.2	0.38	10.6	3.8	0.34	11.3	2.2	0.19
0.85	10.5	4.0	0.36	10.6	3.7	0.33	11.4	1.9	0.16
0.75	10.6	3.8	0.34	10.8	3.4	0.30	11.5	1.7	0.14
0.65	10.7	3.5	0.32	10.9	3.1	0.28	11.5	1.5	0.12
0.55	10.8	3.3	0.29	11.0	2.9	0.25	11.6	1.3	0.10
0.45	11.0	3.0	0.26	11.1	2.5	0.22	11.7	1.1	0.09
0.35	11.1	2.6	0.23	11.3	2.2	0.19	11.8	0.8	0.07
0.25	11.2	2.3	0.19	11.4	1.9	0.15	11.8	0.6	0.05
0.15	11.4	1.9	0.16	11.5	1.5	0.12	11.9	0.4	0.04

Calculated for $\tau_c = 8$, effective radii varying from $r_{base} = 5$ μm to $r_{top} = 12$ μm with an adiabatic profile, $\mu_0 = 0.65$, and a black surface.

μm larger than the measured effective radius. The discrepancy would not be a fault of the retrieval but an artifact of using in situ data from single-level measurements in validating retrievals from a vertically structured cloud. The discrepancy would of course depend significantly on the cloud optical thickness and droplet size profile. Effective radius measurements made at other cloud levels would differ from the 1.6 and 2.2 μm band retrievals as well. As the viewing and/or solar zenith angle increases, the cloud level consistent with the retrievals moves toward cloud top. Therefore a second observation is that for large zenith angles it may be difficult to measure droplet sizes in the very upper regions of the cloud as needed for validation. This is especially true for comparison with 3.7 μm band retrievals where validation requires in situ measurements in the upper 10% of the cloud for $\mu \leq 0.55$.

5.3. Liquid Water Path Estimates

An estimate of liquid water path (LWP) can be made from optical thickness and effective radius retrievals. Combining (1) and (2) yields LWP $\approx 2\tau r_e/3$ (effective radius in micrometers, liquid water path in gm^{-2}). The calculation is strictly valid only for homogeneous clouds having a constant droplet size at all levels. Previous results can be used to test the accuracy of the formulation for the inhomogeneous clouds of Table 2. Water path calculations are shown in Table 5 for the adiabatic cloud, using size retrievals from Table 3a. Liquid water path retrievals generally overestimate actual water path since retrieved effective radii tend to be larger than the mean geometric cloud droplet size. However, overestimates of the actual water path using 1.6 and 2.2 μm band retrievals are seen to be less than 10% and only about 5% on average. The 3.7 μm band retrievals, having larger retrieved effective radii, overestimate water path by 5–17% and by about 12% on average. As expected, the thicker clouds produce the larger errors. Use of the subadiabatic cloud model (profile A) results in smaller liquid water path retrieval errors than for adiabatic clouds. Cloud profile D retrievals tend to give the largest water path errors with estimates being, on average, about 3, 9, and 20% greater than actual for the 1.6, 2.2, and 3.7 μm band retrievals, respectively; in one case ($\tau_c = 5$), the 1.6 μm band retrieval gives a water path less than the actual. However, as discussed, profiles A and B are considered the most physically realistic for single-layer clouds, while profile D mainly serves to test the weighting formulations under more extreme circumstances. The results suggest that retrievals can provide reasonable estimates of liquid water paths, even for moderately thick vertically inhomogeneous clouds.

5.4. Retrievals in the Presence of a Reflecting Surface

Retrievals and weightings have been presented for clouds overlying a black surface. If downwelling intensity from cloud base can be considered Lambertian, the surface albedo of the ocean in visible and near-infrared bands is relatively small at about 0.04 (assuming that specular Fresnel reflectance is the main component and ignoring surface roughness and sea foam). Land surface albedo may vary widely for these bands [*Kaufman et al.*, 1997]. It is not obvious whether retrievals over a known reflecting surface will differ significantly from retrievals for the same cloud overlying a black surface. The assumption of the surface albedo being known is very important. Error due to imperfect knowledge of the albedo is not being investigated here but rather the impact of the surface on the vertical weighting and size retrieval. It is expected that reflected photons having a scattering with the surface will increase the information contribution of lower layers and tend to reduce the

Table 5. Comparison of Reflectance-Inferred Liquid Water Path (LWP) With the Actual Water Path

Cloud Specifications			Vertical Structure Profile B (Adiabatic)		
τ_c	λ, μm	r_e Cloud Base-Top, μm	r_e^* Retrieval, μm	LWP Retrieval/ Actual	LWP Actual, g m^{-3}
15	1.6	4–10	8.8	1.06	
	2.2		9.3	1.10	89
	3.7		9.9	1.17	
10	1.6	6–15	13.0	1.03	
	2.2		13.6	1.08	88
	3.7		14.5	1.15	
8	1.6	5–12	10.2	1.00	
	2.2		10.7	1.05	57
	3.7		11.4	1.12	
5	1.6	8–12	10.4	1.00	
	2.2		10.7	1.03	37
	3.7		11.2	1.05	

Calculations are for horizontally homogeneous plane-parallel cloud layers with effective radii increasing toward cloud top. Two analytic possibilities for the functional dependence of effective radius on cloud optical depth are considered (see Table 2). Comparisons are for bidirectional reflectance with $\mu_0 = 0.65$, $\mu = 0.85$, and a black surface.

retrieved effective radius (when droplet sizes increase with height). If the difference between retrievals with and without a known reflecting surface are negligible, then (4) is still a useful reflectance weighting.

Reflectance retrievals were made for the clouds of Table 3 overlying Lambertian surface albedos of 0.20, 0.10, and 0.05 for the 1.6, 2.2, and 3.7 μm bands, respectively. The albedos are based on nominal values for measured vegetation scenes [*Kaufman et al.*, 1997]. As before, comparisons are made assuming the optical thickness is known exactly. In nearly all cases, retrievals changed insignificantly in the presence of the known reflecting surface (by less than 0.05 μm). The single exception was the 1.6 μm band retrieval for the cloud with $\tau_c = 8$, which showed a difference of about 0.2 μm for the linear profile (D); the adiabatic profile gave a smaller difference. In general, relatively thick clouds will have enough absorption in the near infrared to effectively hide the surface, and consequently there can be no discernible effect on retrievals. While thinner clouds might allow the surface to impact measurements, smaller relative changes in droplet size with height limit the impact on retrievals. Even a thin cloud, with a rather unlikely larger range in droplet size, can show little effect from the surface. For a cloud with $\tau_c = 3$, $r_{base} = 5$ μm, $r_{top} = 10$ μm (equivalent angles as in Table 3), retrievals made with the reflecting surface differ at most by 0.04 μm compared with the black surface, for all bands and profiles.

These examples suggest that the effect of a known surface albedo (vegetation) on droplet size retrievals from vertically inhomogeneous clouds is negligible. If generally true, calculations of w_m for a cloud overlying a black surface can still be used in estimating retrieved sizes.

5.5. Comments on Transmittance-Inferred Retrievals

Retrievals can be made with modeled transmittances in a manner similar to the reflectance-based retrievals. However, transmittance measurements contain relatively little information regarding droplet size. This is due, in part, to the competing way in which droplet single-scattering albedo and asymmetry parameter vary with effective radius, as discussed in section 2. Two difficulties result. First, the sensitivity of transmittance to effective radius over the expected droplet size range is much smaller than for reflectance. This is a difficulty common to all the near-infrared bands. For example, $|dT/dr_e| \leq 0.005$ in the 2.2 μm band (for $\tau_c > 1$, $r_e = 8$ μm, $\mu = 0.85$, $\mu_0 = 0.65$). In comparison, sensitivity for reflectance, $|dR/dr_e|$, is larger by a factor of 3–8 for the same situation. This implies that successful real-world transmittance retrievals require more accurate measurements and cloud models than reflectance retrievals. Second, and more problematic, transmittance curves do not always monotonically decrease with effective radius for a fixed optical thickness in the 1.6 and 2.2 μm bands. This can result in multiple solutions when attempting transmittance-inferred size retrievals. The problem does not appear to be so significant for the 3.7 μm band, though retrievals are now limited to relatively thin clouds due to the larger droplet absorption. Emission is also a source of difficulty in this band. From a theoretical perspective, with no measurement or model error, we can at least test the effectiveness of the transmittance weighting w'_N for the 3.7 μm band. The approach is identical to the reflectance retrieval. For the thinnest cloud in Table 3a ($\tau_c = 5$) the weighting gives size estimates within about 1 μm of the retrievals for both profiles. Figure 5b shows the transmittance weighting function w'_N for the near-infrared bands as a function of viewing angle for the same cloud of Figure 5a.

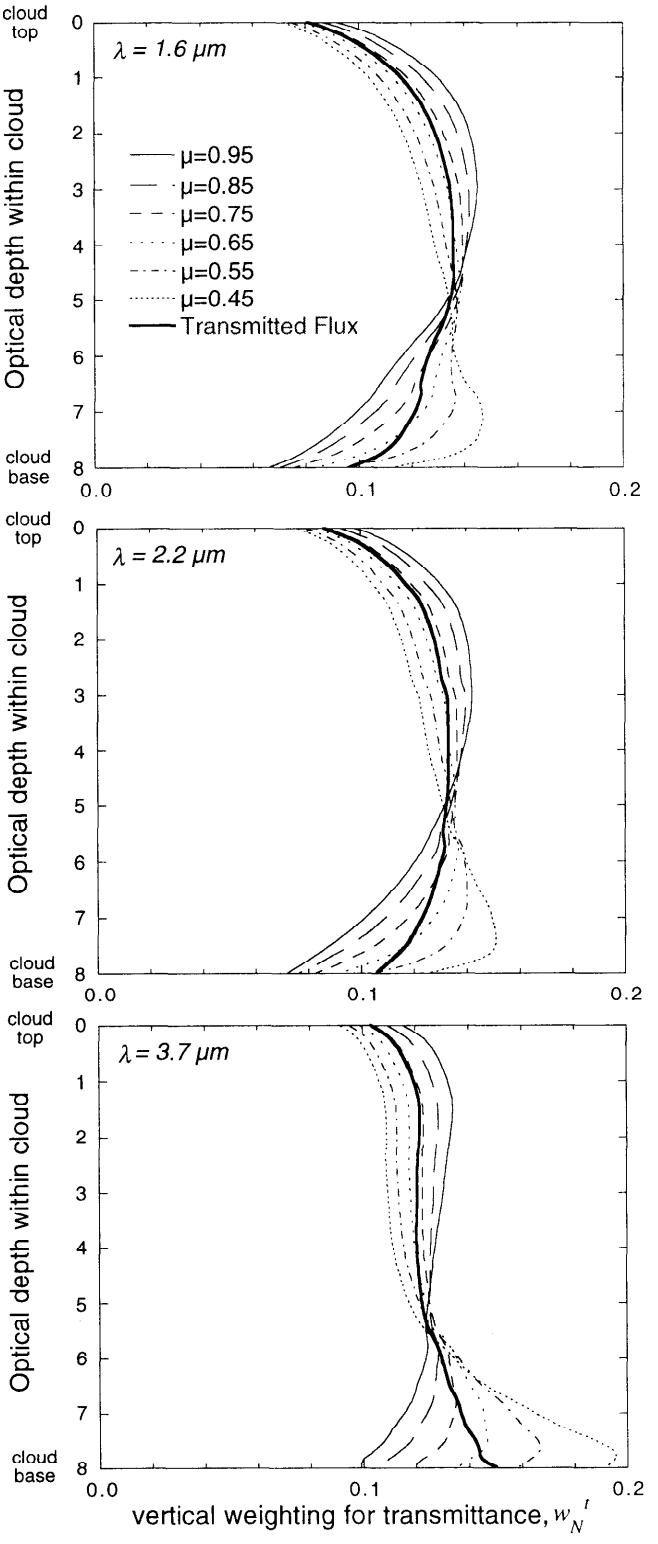

Figure 5b. Same as Figure 5a but for the bidirectional and flux transmittance weighting function w'_N.

5.6. Retrievals Based on Single Scattering

Details of the of the droplet phase function in the backscattered direction can be observed in the glory pattern. This is a

single-scattering phenomenon where differences in scattering angle between brightness peaks of the glory and/or the location of the peaks can be used to estimate droplet size [*Spinhirne and Nakajima*, 1994]. Similarly, polarization patterns observed with the POLDER instrument aboard the ADEOS satellite, also a single-scattering effect, have been used to infer cloud-top droplet sizes [*Descloitres et al.*, 1998]. Droplets contributing to singly scattered radiation will be, on average, located at a depth corresponding to the mean free optical path of reflected photons, which is unity by definition. Representative droplets are therefore located at an optical depth of $(\mu^{-1} + \mu_0^{-1})^{-1}$ (accounting for slant path propagation). This can also be derived from either of the two weighting functions w_m and w'_N, which are equivalent for singly scattered photons. Following (4) the single-scattering contribution to reflectance originating from a differential layer located at a depth τ can be written as $dR(\tau) = \varpi_0 p(\Theta) \exp(-a\tau)\, d\tau$, where $p(\Theta)$ is the scattering phase function at the scattering angle Θ, and $a = \mu^{-1} + \mu_0^{-1}$. Assuming $p(\Theta)$ is constant over the vertical region where $\exp(-a\tau)$ is significant, integration gives the net single-scattering contribution between cloud top and depth τ as $R(\tau) = \varpi_0 p(\Theta) a^{-1}[1 - \exp(-a\tau)]$. The denominator of (4), $R(\tau_c)$, then becomes $\varpi_0 p(\Theta) a^{-1}$ for a cloud optical thickness such that $a\tau_c \gg 1$, and the derivative in the numerator is evaluated as $dR(\tau)/d\tau = \varpi_0 p(\Theta) \exp(-a\tau)$. The ratio gives the weighting for singly scattered reflected radiation as

$$w_{\text{single}}(\tau) = ae^{-a\tau}. \tag{5}$$

The average optical depth $\bar{\tau}$ is given by the first moment of (5), which is a^{-1} as expected. Note that $\bar{\tau} \leq 0.5$ (maximum for overhead solar and viewing angles). This close proximity to cloud top implies that single-scattering retrieval methods will infer larger droplet sizes than the reflectance-inferred retrievals (for droplet size increasing with height), except in the optically thin limit where both are equivalent.

Optical depths corresponding to retrieved effective radii were given in Table 4 for the adiabatic cloud model with $\tau_c = 8$. The table shows those depths to be much greater than the single-scattering mean depth for all bands and viewing angles. For instance, the 2.2 μm band retrieval at $\mu = 0.85$ and $\mu_0 = 0.65$ corresponds to a depth of 3.7 (effective radius of 10.6 μm), whereas the single-scattering depth is 0.37 (effective radius of about 12 μm, corresponding to a geometric depth of less than 10 m for this example). It is practically impossible to obtain statistically meaningful in situ measurement of droplet sizes this close to cloud top where significant entrainment from above is probable. Single-scattering methods might therefore provide a practical method for studying cloud-top microphysical processes.

5.7. Weighting Functions for Emission

Cloud thermal emission can be a significant, and sometimes dominant part of the total measured intensity in the 3.7 μm band. For example, a uniform cloud that is optically thick at this wavelength ($\tau_c \approx 6$), with an effective radius of 10 μm and a temperature of 290 K, emits radiation that is roughly equivalent to the reflected solar radiation. Larger effective radii would have greater droplet absorption, thereby increasing cloud emissivity and emission, and decreasing cloud reflectance or transmittance. Reflectance-based retrieval algorithms compare the total upwelling 3.7 μm measured intensity with reflectance and emissivity libraries calculated from homogeneous cloud models. It is not obvious that emitted and solar reflected (or transmitted) 3.7 μm radiation in vertically structured clouds would be represented by the same homogeneous cloud effective radius. Emission is further complicated by a potentially significant thermal structure. Analogous to the previous use of vertical weighting functions in solar scattering problems, we seek a function such that (3) approximates the effective radius of a homogeneous cloud having the same emission as the vertically inhomogeneous cloud. We denote this vertical weighting function as $w_e(\tau, \tau_c, \mu)$ corresponding to emission in the viewing direction μ. In general, for a vertically structured cloud, two separate weighting functions will be needed to describe emission transported to both cloud base and cloud top boundaries. In the following discussion, we use a single notation for both.

A straightforward candidate weighting for emission is one proportional to the amount that a differential layer contributes to the overall emitted intensity, i.e., a weighting defined such that $w_e(\tau, \tau_c, \mu)\, d\tau$ gives the radiation emerging at a cloud boundary in the direction μ, due to photons emitted in all directions from a layer of thickness $d\tau$, located at a depth τ, in a cloud of optical thickness τ_c. The normalization of this weighting is therefore the net cloud emission in the direction μ. The weighting is derived by first determining layer emission and then accounting for transport to the boundaries. Radiation emitted by a differential layer is $B(T)\, d\tau(1 - \varpi_0)/\mu$, where $d\tau(1 - \varpi_0)/\mu$ is the layer emissivity, $B(T)$ is the Planck function, T is the temperature of the layer, and ϖ_0 is the layer's single-scattering albedo. It is understood that all scattering and emission quantities are a function of wavelength and position. Transport of layer emission to the cloud boundaries is then obtained from the escape operators, or escape matrices in the present numerical implementation. A discussion of escape operators in homogeneous emission problems and some examples are given by *Twomey* [1979]. Modifications to vertically inhomogeneous layers are straightforward.

For low-level adiabatic clouds, temperature decreases approximately linearly with height up to several kilometers in thickness. For a cloud 300 m thick (considered in Table 2) the temperature difference between cloud base and cloud top would only be a couple of degrees Kelvin. A subadiabatic cloud may be expected to have an even smaller lapse rate. In the 3.7 μm band, $\Delta T = 2$ K corresponds to less than a 10% difference in the Planck radiance for warm clouds. For such cases we can consider the clouds to be isothermal to first order. With $B(T)$ a constant the proposed emission weighting reduces to the effective emissivity of the layer as observed from cloud top or base. Since $1 - \varpi_0$ is approximately proportional to effective radius for cloud droplets in the near infrared [*Twomey and Bohren*, 1980], replacing the weighting's $d\tau(1 - \varpi_0)/\mu$ layer emissivity term with $d\tau/\mu$ would appear to give a weighting more appropriate for use in (3). The following examples suggest that this modification does help in describing cloud-top emission when modeled cloud effective radii decrease with height but that the original weighting definition using layer emissivity works better when effective radii increase with height. This indicates that neither of the two weightings are exact in the sense of (3). Still, they provide an adequate approximation, as demonstrated below.

Cloud-top vertical emission weightings for the 3.7 μm band were determined for four isothermal clouds with the vertical structure described in Table 2. The weightings were then used

Table 6a. Comparison of 3.7 μm Reflectance-Inferred Effective Radius Retrievals (Table 3a) With That of Emission for an Isothermal Cloud

Cloud Specifications			Vertical Structure					
			Profile *D*			Profile *B* (Adiabatic)		
τ_c	λ, μm	r_e Cloud Base-Top, μm	r_e^* Reflectance-Only Retrieval, μm	r_e^* Emission-Only Retrieval, μm	r_e^* w_e Estimate, μm	r_e^* Reflectance-Only Retrieval, μm	r_e^* Emission-Only Retrieval, μm	r_e^* w_e Estimate, μm
15	3.7	4–10	9.4	9.1	8.7	9.9	9.8	9.6
10	3.7	6–15	13.4	13.0	12.5	14.5	14.2	13.9
8	3.7	5–12	10.5	10.1	9.8	11.4	11.2	11.0
5	3.7	8–12	10.9	10.8	10.6	11.2	11.1	10.9

Retrievals corresponding to reflectance are the droplet size of a homogeneous cloud having a bidirectional reflectance equivalent to that of the vertically structured cloud. Retrievals corresponding to emission are the droplet size of a homogeneous cloud giving an emissivity equivalent to that of the vertically structured cloud; an estimate of this radius using an emission weighting w_e proportional to $(1 - \varpi_0)\, d\tau/\mu_i$ with equation (3) is also shown. Calculations are for horizontally homogeneous plane-parallel cloud layers with effective radii increasing toward cloud top. Comparisons are for $\mu_0 = 0.65$, $\mu = 0.85$, and a black surface.

in (3) to approximate the effective radius of a homogeneous cloud having the same cloud-top emission as the vertically structured cloud. Results are summarized in Table 6a for r_e increasing with height, when using the weighting proportional to layer emissivity. Table 6b gives results using the modified weighting for r_e decreasing with height (same situation as cloud base emission when r_e increases with height). Also shown is the droplet size inferred by matching calculations of homogeneous cloud-top emission with the vertically structured cloud emission. This is analogous to a reflectance-based effective radius retrieval and is referred to in the table as the emission-only retrieval. Potential surface emission transmitted through the cloud is ignored. The weighting-derived effective radii are generally within several tenths of a micron of the retrieved size for the adiabatic clouds and typically better than half a micron for clouds specified by effective radius linear with optical depth.

For comparison, Tables 6a and 6b also give reflection-inferred effective radius retrievals, referred to as reflectance-only retrieval (from Table 3). The encouraging conclusion is that reflectance and emission-inferred effective radii retrievals for all modeled clouds are, on average, within 0.2 μm of each other, with a maximum difference of 0.4 μm; the maximum difference is just 0.2 μm for the adiabatic cloud models. We conclude that for the 3.7 μm band, a consistent effective radius is likely to represent both reflectance and emitted radiation in vertically structured clouds. If this were not the case, retrieved radii would lie somewhere between the reflectance-inferred and emission-inferred sizes, depending on cloud temperature and structure. These results are somewhat remarkable given the difference in the emission and reflectance vertical weighting functions. An example is shown in Figure 6.

The emission weighting function discussed in this section should also prove useful for studying cloud particle size retrievals using longer wavelengths, such as the 8.5, 10, and 11 μm bands [*Ackerman et al.*, 1998] and in comparing size information from those algorithms with solar scattering methods.

6. Information Regarding the Droplet Size Profile

To the extent that the retrieved effective radius varies with each near-infrared band in the examples of Table 3, there is evidently some information regarding the droplet size profile that may be inferred from the three retrievals. The weighting function plots of Figure 5a also demonstrate that each near-infrared band is sampling the cloud layers in different proportions, suggesting the possibility of an inversion for the size profile. However, the relatively monotonic nature of the functions, except for a small maximum near cloud top, makes them less than optimum for inversions. A quantitative assessment of the information content in the three reflectance-based retrievals will be discussed in this section. It is the information content that is of immediate interest. Implementation and testing

Table 6b. Same as Table 6a but for Plane-Parallel Cloud Layers With Effective Radii Decreasing Toward Cloud Top and an Emission Weighting w_e Proportional to $d\tau/\mu_i$

Cloud Specifications			Vertical Structure					
			Profile *D*			Profile *B* (Adiabatic)		
τ_c	λ, μm	r_e Cloud Base-Top, μm	r_e^* Reflectance-Only Retrieval, μm	r_e^* Emission-Only Retrieval, μm	r_e^* w_e Estimate, μm	r_e^* Reflectance-Only Retrieval, μm	r_e^* Emission-Only Retrieval, μm	r_e^* w_e Estimate, μm
15	3.7	10–4	4.8	5.1	5.2	4.0	4.2	4.2
10	3.7	15–6	7.5	7.6	8.4	6.2	6.3	6.5
8	3.7	12–5	6.5	6.8	7.1	5.2	5.4	5.5
5	3.7	12–8	9.2	9.4	9.6	8.5	8.6	8.8

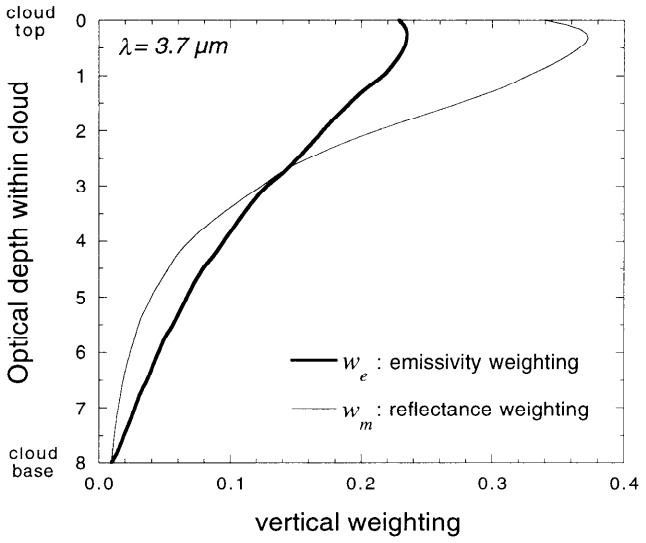

Figure 6. Example of normalized reflectance and cloud-top emissivity weightings for a 3.7 μm spectral channel. Calculated for the same profile, microphysical boundary conditions, and geometry of Figure 2. Though the curves are significantly different, the weighting-derived effective radius (equation (3)) differs by only a few tenths of a micron.

of an actual inversion algorithm is not undertaken. Ultimately, the usefulness and required accuracy of an inversion depends on the intended application (e.g., improvement in liquid water path estimates, cloud process studies, etc.).

At most, three pieces of unique information regarding the profile shape can be acquired from the three retrievals. However, both the figure and the retrieval results make it clear that there is relatively little difference in the information content of the 1.6 and 2.2 μm bands. There will be an obvious difficulty in realizing unique information from both these bands when differences between the two retrievals are less than the retrieval uncertainty. For such a case, information is effectively limited to two pieces of information. Retrieval uncertainty can be present in the form of measurement error, error in weighting function effective radius estimates, and numerical error. The eigenvalues of the covariance, or correlation, matrix are a useful indication of the number of pieces of information provided by the three weightings in the presence of error. The elements of this symmetric matrix, $C_{i,j}$, are given by the inner product of the weightings (the weighting functions are equivalent to the kernels in inversion theory). For example, we can let $C_{1,2} = \int_0^{\tau_c} w_{1.6}(\tau, \tau_c) w_{2.2}(\tau, \tau_c)\, d\tau$, where the indices 1 and 2 refer to the 1.6 and 2.2 μm weightings, respectively. Likewise, index 3 will refer to the 3.7 μm band. It is useful to normalize the retrieval equation (equation (3)) by r_e^* which, in turn, scales the covariance matrix ($C_{i,j} \rightarrow C_{i,j}/r_{ei}^* r_{ej}^*$). Let e_r represents the relative error in retrieving r_e^* (assumed constant in all bands). Then for all weightings to contribute unique information, the minimum eigenvalue of the scaled covariance matrix must be greater than about e_r^2/Nr_m^2, where N is the number of measurements and r_m is the mean value of the unknown $r_e(\tau)$ profile [*Twomey*, 1977].

As an example, consider the cloud specified by $\tau_c = 8$, $r_{\text{base}} = 5$ μm, $r_{\text{top}} = 12$ μm, with an adiabatic profile (Table 3a). The value of r_m is about 10 μm for this cloud. It is doubtful that typical relative retrieval errors can be expected to be better than 5% in any band (due to limitations in cloud model library calculations and instrument uncertainty). Furthermore, the 1.6 μm band weighting function gave about 2.5% error in the retrieval estimate for this cloud (Table 3a); weighting function errors in the other bands were about 1% or less. The combination of retrieval and weighting function error suggests a relative error in the range of 5–10%. Therefore the minimum eigenvalues of the scaled covariance matrix need to be greater than about 8×10^{-6} to 30×10^{-6} for this example if each retrieval is to add information. It was found that the smallest eigenvalue (1×10^{-6}) is less than these limits, implying that only two pieces of information are available regarding the size profile. The 0.1 μm difference between 1.6 and 2.2 μm weighting-derived retrieval estimates (Tables 3a, 4) conveys the same conclusion. Some improvement can be obtained by using different viewing angles for each band, for example, from low-level aircraft measurements. As shown in Figure 5a, the peak in the weighting function moves toward cloud top and narrows as viewing zenith angle increases. The previous example was repeated with a viewing geometry of $\mu = 0.95$, 0.65, and 0.45 for the 1.6, 2.2, and 3.7 μm bands, respectively. After scaling, the minimum eigenvalue is now 32×10^{-6}. This implies that three pieces of information might be possible for 5% relative error but probably only two pieces for 10% relative error. This is in accord with expectations from the retrieval results (Table 4), where the 1.6 and 2.2 μm retrieval size difference is 0.5 μm, or about 5%. The analysis is for one particular case. Results will vary with cloud thickness, effective radius profile, and available geometry. However, similar conclusions occurred for other profiles and clouds from Table 2.

If three pieces of information are possible, it is not clear which three pieces are feasible. For instance, we could attempt to retrieve the three parameters a_0, a_1, and x in the analytic formula for the effective radius profile given in Table 1. As an alternative, $r_e(\tau)$ could be described by the three coefficients of a second-order polynomial. Though a quadratic is adequate for approximating profiles C and D of Figure 1, a third-order polynomial is required to sufficiently approximate a typical adiabatic profile. However, a quadratic form simplifies the quadrature of (3), giving the retrieved radius in any near-infrared band in terms of moments of the weighting function (i.e., $r_e^* = \alpha_0 + \alpha_1 \bar{\tau} + \alpha_2 \bar{\tau^2}$, where the α values are unknown coefficients of the quadratic fit, $\bar{\tau}$ is the first moment of $w_m(\tau, \tau_c)$, etc.). Retrieval estimates for each band can then be expressed in matrix form by the rows of the equation $\mathbf{r}_e^* = \mathbf{A}\alpha$, where α is the unknown vector, $\mathbf{r}_e^*$ constitutes the measurement vector, and the matrix $\mathbf{A}$ contains the moments. Other profile retrieval alternatives include the effective radii in three layers of specified depth, or the effective radii in two layers of variable depth. If only two pieces of information are possible, a linear fit to the size profile might be retrieved (a physically improbable profile, as previously discussed) or, alternatively, the effective radii in two layers of fixed depth.

Equation (3) for the weighting-derived retrieved droplet size estimate appears similar to a Fredholm integral of the first kind, an integral form which serves as a basis for a wide range of atmospheric inversion problems [*Twomey*, 1977]. However, the kernel in this equation is the maximum penetration weighting w_m which, though not explicitly indicated above, is also a function of the unknown profile $r_e(\tau)$. The resulting nonlinearity between retrievals and the unknown precludes the use of a constrained linear inversion unless a linearized form of the equation, with a constant weighting function (e.g., derived

from a nominal profile), proves satisfactory. Otherwise, an iterative approach is required.

In summary, the ability of three separate near-infrared band retrievals to infer three unique pieces of information regarding the droplet size profile is problematic at a fixed viewing angle (at least for the cloud example considered). It is probable that such an inversion would be limited to two pieces of information. The use of multiple-viewing angles allows for the possibility of obtaining a third piece of information.

7. Discussion and Conclusions

Cloud optical thickness and effective radius remote sensing retrievals make use of measurements in visible and near-infrared atmospheric window bands (at 1.6, 2.2, and 3.7 μm), with the water-absorbing near-infrared bands containing the size information. Retrieval algorithms compare measurements with look-up tables calculated from plane-parallel, homogeneous cloud models. The implication is that either observed clouds can be considered approximately homogeneous for retrieval purposes, i.e., cloud structure has little influence on retrievals, or that the retrieval is understood to be the plane-parallel, homogeneous equivalent value. If clouds have a vertical structure, then separate near-infrared band retrievals may infer different effective radii, a situation that has been observed in airborne radiometer data [*Platnick et al.*, 2000]. We have relaxed the vertical homogeneity constraint in this paper and looked at the effect of modeled vertical droplet size profiles on retrieved effective radii.

Analytic effective radius profiles were developed for clouds that are subadiabatic at upper levels, adiabatic clouds, and two cloud models with drying at midlevels. The maximum cloud optical thickness considered was 15. For the adiabatic profiles, absolute differences between 1.6 and 2.2 μm retrievals are typically half a micrometer or less, about the same size as the minimum expected retrieval error; 3.7 μm retrievals are larger than for either of these bands (by almost 1 μm). Retrievals provided reasonably good liquid water path estimates for the adiabatic cloud models, overestimating by about 5% on average for 1.6 and 2.2 μm retrievals and 12% for 3.7 μm retrievals; water path errors increase with optical thickness (all else being equal). In summary, adiabatic cloud retrievals showed relatively minor influences due to the vertical structure of cloud droplet effective radius. Clouds that are subadiabatic at upper levels give retrieval results that are even more homogeneous-like. Multilayer cloud systems (or models with midlevel drying) are likely to have the most significant retrieval signatures.

Several vertical weighting functions were proposed for approximating the retrieved size. The most accurate weighting for reflectance-based retrievals was one based on maximum photon penetration. This weighting was able to predict retrieved radii from the various vertically inhomogeneous cloud models to within a tenth of a micrometer for the 2.2 and 3.7 μm bands and within a third of a micrometer for the less absorbing 1.6 μm band. Retrievals from glory or polarization single-scattering reflectance patterns infer droplet sizes from the very uppermost region of the cloud (within meters of cloud top) and thus may be substantially different from total reflectance retrievals (dominated by multiple scattering). For the same reason, single-scattering retrievals would be difficult, if not impossible, to validate. In addition to providing information regarding the scale of vertical transport, the weightings provide a means for investigating and understanding the possibility of an inversion for the droplet size profile using the three near-infrared size retrievals. Analysis shows that the most probable possibility for realizing three unique pieces of information from the retrievals is through the use of multiple-viewing angles.

Though the emphasis of this work has been on multiple-scattering weighting functions for liquid water clouds, the derived weightings should be useful for other multiple-scattering plane-parallel radiative transfer problems, including arbitrary combinations of cloud (liquid or ice particles), aerosol, and gas layers.

Acknowledgments. This work was supported in part by grant NAG5-6996 from the National Aeronautics and Space Administration, EOS validation program office. The author wishes to thank D. Flittner, R. Pincus, and S. Twomey for helpful discussions, and comments from two anonymous reviewers.

References

Ackerman, S. A., W. L. Smith, A. D. Collard, X. L. Ma, H. E. Revercomb, and R. O. Knuteson, Cirrus cloud properties derived from high spectral resolution infrared spectrometry during FIRE II, part II, Aircraft HIS results, *J. Atmos. Sci.*, *52*, 4246–4263, 1995.

Ackerman, S. A., C. C. Moeller, K. I. Strabala, H. E. Gerber, L. E. Gumley, W. P. Menzel, and S. C. Tsay, Retrieval of effective microphysical properties of clouds: A wave cloud case study, *Geophys. Res. Lett.*, *25*, 1121–1124, 1998.

Albrecht, B. A., Aerosols, cloud microphysics, and fractional cloudiness, *Science*, *245*, 1227–1230, 1989.

Arking, A., and J. D. Childs, Retrieval of cloud cover parameters from multispectral satellite images, *J. Clim. Appl. Meteorol.*, *24*, 322–333, 1985.

Austin, P., Y. Wang, R. Pincus, and V. Kujala, Precipitation in stratocumulus clouds: Observational and modeling results, *J. Atmos. Sci.*, *52*, 2329–2352, 1995.

Cahalan, R. F., and J. B. Snider, Marine stratocumulus structure, *Remote Sens. Environ.*, *28*, 95–107, 1989.

Chandrasekhar, S., *Radiative Transfer*, 393 pp., Dover, Mineola, N. Y., 1960.

Charlson, R. J., J. E. Lovelock, M. O. Andreae, and S. G. Warren, Oceanic phytoplankton, atmospheric sulfur, cloud albedo and climate, *Nature*, *326*, 655–661, 1987.

Curry, J. A., Interactions among turbulence, radiation, and microphysics in arctic stratus clouds, *J. Atmos. Sci.*, *43*, 90–106, 1986.

Descloitres, J., J. C. Buriez, F. Parol, and Y. Fouquart, POLDER observations of cloud bidirectional reflectances compared to a plane-parallel model using the International Satellite Cloud Climatology Project cloud phase function, *J. Geophys. Res.*, *103*, 11,411–11,418, 1998.

Foot, J. S., Some observations of the optical properties of cloud, part I, Stratocumulus, *Q. J. R. Meteorol. Soc.*, *114*, 129–144, 1988.

Garrett, T. J., and P. V. Hobbs, Long-range transport of continental aerosols over the Atlantic Ocean and their effects on cloud structure, *J. Atmos. Sci.*, *52*, 2977–2984, 1995.

Gerber, H., B. G. Arends, and A. S. Ackerman, New microphysics sensor for aircraft use, *Atmos. Res.*, *31*, 235–252, 1994.

Han, Q., W. B. Rossow, and A. A. Lacis, Near-global survey of effective droplet radii in liquid water clouds using ISCCP data, *J. Clim.*, *7*, 465–497, 1994.

Han, Q., W. Rossow, R. Welch, A. White, and J. Chou, Validation of satellite retrievals of cloud microphysics and liquid water path using observations from FIRE, *J. Atmos. Sci.*, *52*, 4183–4195, 1995.

Kaufman, Y. J., A. E. Wald, L. A. Remer, B.-C. Gao, R.-R. Li, and L. Flynn, The MODIS 2.1-μm channel—Correlation with visible reflectance for use in remote sensing of aerosol, *IEEE Trans. Geosci. Remote Sens.*, *35*, 1286–1298, 1997.

Kiehl, J. T., Sensitivity of a GCM climate simulation to differences in continental versus maritime cloud drop size, *J. Geophys. Res.*, *99*, 23,107–23,115, 1994.

King, M. D., Y. J. Kaufman, W. P. Menzel, and D. Tanre, Remote-sensing of cloud, aerosol, and water-vapor properties from the Mod-

erate Resolution Imaging Spectrometer (MODIS), *IEEE Trans. Geosci. Remote Sens.*, *30*, 2–27, 1992.

Martin, G. M., D. W. Johnson, and A. Spice, The measurement and parameterization of effective radius of droplets in warm stratocumulus clouds, *J. Atmos. Sci.*, *51*, 1823–1842, 1994.

McFarquhar, G. M., and A. J. Heymsfield, The definition and significance of an effective radius for ice clouds, *J. Atmos. Sci.*, *55*, 2039–2052, 1998.

Nakajima, T., and M. D. King, Determination of the optical thickness and effective particle radius of clouds from reflected solar radiation measurements, I, Theory, *J. Atmos. Sci.*, *47*, 1878–1893, 1990.

Nakajima, T., M. D. King, J. D. Spinhirne, and L. F. Radke, Determination of the optical thickness and effective particle radius of clouds from reflected solar radiation measurements, II, Marine stratocumulus observations, *J. Atmos. Sci.*, *48*, 728–750, 1991.

Nicholls, S., and J. Leighton, An observational study of the structure of stratiform cloud sheets, part I, Structure, *Q. J. R. Meteorol. Soc.*, *112*, 431–460, 1986.

Noonkester, V. R., Droplet spectra observed in marine stratus cloud layers, *J. Atmos. Sci.*, *41*, 829–845, 1984.

Ou, S. C., K. N. Liou, Y. Takano, N. X. Rao, Q. Fu, A. J. Heymsfield, L. M. Miloshevich, B. Baum, and S. A. Kinne, Remote sounding of cirrus cloud optical depths and ice crystal sizes from AVHRR data: Verification using FIRE II IFO measurements, *J. Atmos. Sci.*, *52*, 4143–4158, 1995.

Parol, F., J. C. Buriez, G. Brogniez, and Y. Fouquart, Information content of AVHRR channels 4 and 5 with respect to the effective radius of cirrus cloud particles, *J. Appl. Meteorol.*, *30*, 973–984, 1991.

Pincus, R., and M. B. Baker, Effect of precipitation on the albedo susceptibility of clouds in the marine boundary layer, *Nature*, *372*, 250–252, 1994.

Platnick, S., The scales of photon transport in cloud remote sensing problems, in *IRS '96: Current Problems in Atmospheric Radiation*, edited by W. L. Smith and K. Stamnes, pp. 206–209, A. Deepak, Hampton, Va., 1997.

Platnick, S., Approximations for horizontal photon transport in cloud remote sensing problems, *J. Quant. Spectrosc. Radiat. Transfer*, in press, 2000a.

Platnick, S., A superposition technique for deriving mean photon scattering statistics in plane-parallel cloudy atmospheres, *J. Quant. Spectrosc. Radiat. Transfer*, in press, 2000b.

Platnick, S., and S. Twomey, Determining the susceptibility of cloud albedo to changes in droplet concentrations with the Advanced Very High Resolution Radiometer, *J. Appl. Meteorol.*, *33*, 334–347, 1994.

Platnick, S., and F. P. J. Valero, A validation of a satellite cloud retrieval during ASTEX, *J. Atmos. Sci.*, *52*, 2985–3001, 1995.

Platnick, S., P. A. Durkee, K. Nielsen, J. P. Taylor, S.-C. Tsay, M. D. King, R. J. Ferek, P. V. Hobbs, and J. W. Rottman, The role of background cloud microphysics in the radiative formation of ship tracks, *J. Atmos. Sci.*, *57*, 2607–2624, 2000.

Rawlins, F., and J. S. Foot, Remotely sensed measurements of stratocumulus properties during FIRE using the C130 aircraft multichannel radiometer, *J. Atmos. Sci.*, *47*, 2488–2503, 1990.

Slingo, A., Sensitivity of the Earth's radiation budget to changes in low clouds, *Nature*, *343*, 49–51, 1990.

Slingo, A., S. Nicholls, and J. Schmetz, Aircraft observations of marine stratocumulus during JASIN, *Q. J. R. Meteorol. Soc.*, *108*, 833–856, 1982.

Spinhirne, J. D., and T. Nakajima, Glory of clouds in the near-infrared, *Appl. Opt.*, *33*, 4652–4662, 1994.

Stephens, G. L., and C. M. R. Platt, Aircraft observations of the radiative and microphysical properties of stratocumulus and cumulus cloud fields, *J. Clim. Appl. Meteorol.*, *26*, 1243–1269, 1987.

Twomey, S., Pollution and the planetary albedo, *Atmos. Environ.*, *8*, 1251–1256, 1974.

Twomey, S., *Introduction to the Mathematics of Inversion in Remote Sensing and Indirect Measurements*, 243 pp., Dover, Mineola, N. Y., 1977.

Twomey, S., Doubling and superposition methods in the presence of thermal emission, *J. Quant. Spectrosc. Radiat. Transfer*, *22*, 355–363, 1979.

Twomey, S., Aerosols, clouds, and radiation, *Atmos. Environ.*, *25A*, 2435–2442, 1991.

Twomey, S., and C. F. Bohren, Simple approximations for calculations of absorption in clouds, *J. Atmos. Sci.*, *37*, 2086–2094, 1980.

Twomey, S., and T. Cocks, Spectral reflectance of clouds in the near-infrared: Comparison of measurements and calculations, *J. Meteorol. Soc. Jpn.*, *60*, 583–592, 1982.

Twomey, S., and T. Cocks, Remote sensing of cloud parameters from spectral reflectance measurements in the near-infrared, *Beitr. Phys. Atmos.*, *62*, 172–179, 1989.

Twomey, S., H. Jacobowitz, and H. B. Howell, Matrix methods for multiple scattering problems, *J. Atmos. Sci.*, *23*, 101–108, 1966.

Wielicki, B. A., R. D. Cess, M. D. King, D. A. Randall, and E. F. Harrison, Mission to Planet Earth—Role of clouds and radiation in climate, *Bull. Am. Meteorol. Soc.*, *76*, 2125–2153, 1995.

Young, D. F., P. Minnis, D. Baumgardner, and H. Gerber, Comparison of in situ and satellite-derived cloud properties during SUCCESS, *Geophys. Res. Lett.*, *25*, 1125–1128, 1998.

S. Platnick, NASA GSFC, Code 913, Greenbelt, MD 20771. (platnick@climate.gsfc.nasa.gov)

(Received September 3, 1999; revised May 1, 2000; accepted May 15, 2000.)